UC Irvine
UC Irvine Previously Published Works

Title
Prolonged rod photoresponse and enhanced cone sensitivity in the transgenic mouse retina lacking arrestin and guanylate cyclase activating proteins

Permalink
https://escholarship.org/uc/item/42p9g2js

Journal
The Journal of Physiology

ISSN
0022-3751

Authors
Sato, Shinya
Frederiksen, Rikard
Sampath, Alapakkam P
et al.

Publication Date
2026-10-28

DOI
10.1113/jp291252

Copyright Information
This work is made available under the terms of a Creative Commons Attribution License, available at https://creativecommons.org/licenses/by/4.0/

Peer reviewed

eScholarship.org Powered by the California Digital Library
University of California

Check for updates

The Journal of Physiology

J Physiol 604.22 (2026) pp 9073–9094

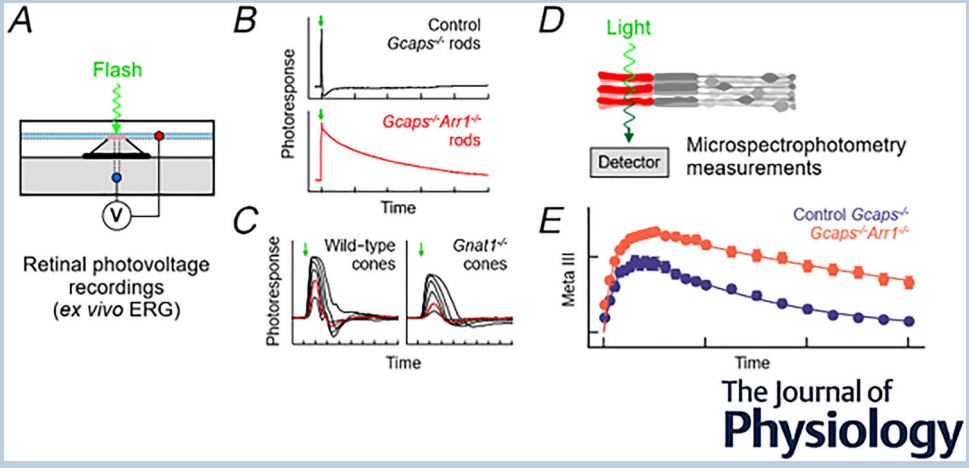
Prolonged rod photoresponse and enhanced cone sensitivity in the transgenic mouse retina lacking arrestin and guanylate cyclase activating proteins

Shinya Sato[1], Rikard Frederiksen[2], Alapakkam P. Sampath[2] and Vladimir J. Kefalov[1,3]

[1]*Department of Ophthalmology and Visual Sciences, Gavin Herbert Eye Institute –Brunson Center for Translational Vision Research, University of California, Irvine, California, USA*
[2]*Jules Stein Eye Institute, David Geffen School of Medicine, University of California, Los Angeles, California, USA*
[3]*Department of Physiology and Biophysics, University of California, Irvine, California, USA*

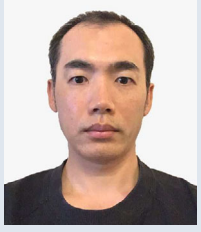
Handling Editors: Jing-Ning Zhu & Nathan Schoppa

The peer review history is available in the Supporting Information section of this article (https://doi.org/10.1113/JP291252#support-information-section).



Abstract figure legend Analyses from mutant mouse retinal explants gives invaluable insights of the photosignaling process in rod and cone photoreceptor cells. A, Illustration of retinal photovoltage recordings. A retinal explant (pink) is placed in a transparent device which has electrodes to monitor transretinal voltage (red and blue circles). B, Retinas from newly established *Gcaps*$^{-/-}$*Arr1*$^{-/-}$ mutant mice showed 100 times slower rod photoresponse (red) than control *Gcaps*$^{-/-}$ retinas (black). C. Cone response families of wild type mice and *Gnat1*$^{-/-}$ mice, which lack rod signaling. Larger responses in wild type cones suggests potentiation of cones by rod signaling. D, Illustration of the microspectrophotometry measurement. The light is focused on rod outer segments (red) sticking out from the retinal fragment. Formation and decay of photoactivated intermediates of rhodopsin are analyzed in situ based on

Shinya Sato earned a PhD from Osaka University in Japan for research on carp cone photoreceptor cells (2014). He then completed postdoctoral training at Washington University in St. Louis (USA), where he conducted electrophysiological studies on isolated rod and cone photoreceptors and retinal explants (2014–17). He subsequently served as an Assistant Professor at Kyoto University (2017–21), Laboratory Chief at the National Cerebral and Cardiovascular Center (2021–22), and Project Scientist at UC Irvine (2023–26). Throughout his career, he has investigated the function of rods and cones in carp, salamander, bullfrog, mouse and zebrafish retinas using biochemical, electrophysiological and live imaging approaches.



© 2026 The Author(s). *The Journal of Physiology* published by John Wiley & Sons Ltd on behalf of The Physiological Society.

DOI: 10.1113/JP291252

This is an open access article under the terms of the Creative Commons Attribution License, which permits use, distribution and reproduction in any medium, provided the original work is properly cited.

their characteristic absorption spectra. E, The Meta III form of photoactivated rhodopsin showed slower decay in *Gcaps*$^{-/-}$*Arr1*$^{-/-}$ rods.

Abstract Light activates visual pigments and downstream G protein signalling cascades in rod and cone photoreceptor cells. Timely response inactivation requires visual pigment inactivation by arrestin and restoration of cellular cGMP by guanylate cyclase activating proteins (GCAPs). Using GCAP-deficient mice, we previously showed that apo-opsin produces photoresponse-like signals. To investigate the inactivation of apo-opsin by arrestin, we generated GCAP-deficient mice lacking arrestin (*Gcaps*$^{-/-}$*Arr1*$^{-/-}$). Using *ex vivo* electroretinography, we found that the dim flash responses of *Gcaps*$^{-/-}$*Arr1*$^{-/-}$ rods were ∼100-fold slower than those of control *Gcaps*$^{-/-}$ rods. As a result, even brief dim light exposure during sample preparation resulted in prolonged rod saturation, so that only cone responses were initially observed in *Gcaps*$^{-/-}$*Arr1*$^{-/-}$ retinas. In contrast, rod responses were observed immediately when *Gcaps*$^{-/-}$*Arr1*$^{-/-}$ retinas were dissected under infrared light to avoid rod photoactivation. Microspectrophotometry showed that the rate of production and decay of the active rhodopsin photoproduct, Meta II, was comparable between *Gcaps*$^{-/-}$ and *Gcaps*$^{-/-}$*Arr1*$^{-/-}$ rods. However, the rate of photoproduct Meta III decay was 3-fold slower in *Gcaps*$^{-/-}$*Arr1*$^{-/-}$ rods, supporting a role for arrestin in accelerating the decay of photoactivated rhodopsin. To evaluate the effect of rod saturation on cone responses, we compared photopic cone responses from wild-type and *Gnat1*$^{-/-}$ retinas lacking rod signalling. Cone photoresponses were larger and more sensitive in wild-type retinas, suggesting the potentiation of cone function by the saturation of rod phototransduction. Together, our results demonstrate that the very slow deactivation of rod responses in *Gcaps*$^{-/-}$*Arr1*$^{-/-}$ retinas might result in selective and potentiated cone signalling in darkness.

(Received 23 February 2026; accepted after revision 25 September 2026; first published online 28 October 2026)
Corresponding author V. Kefalov: Department of Ophthalmology and Visual Sciences, Gavin Herbert Eye Institute, University of California, Irvine 847 Health Sciences Road, Irvine, CA 92617, USA. Email: vkefalov@hs.uci.edu

Key points

- Arrestin and guanylate cyclase activating proteins (GCAPs) play an important role in inactivation of the phototransduction cascade and termination of the light response in rod photoreceptors.
- The deletion of arrestin and GCAPs results in ∼100-fold slower dim flash responses in rods so that even brief dim light exposure produces saturation of the rods for tens of minutes.
- The decay of the rhodopsin photoactivated intermediate Meta III was slowed down 3-fold by the deletion of arrestin in *Gcaps*$^{-/-}$ rods, supporting a role for arrestin in accelerating the decay of photoactivated rhodopsin.
- Cone photoresponses were smaller and less sensitive in retinas lacking rod signalling, suggesting potentiation of cone function by the saturation of rod phototransduction.
- Together, these results demonstrate that the very slow deactivation of rod responses in arrestin- and GCAP-deficient retinas can result in selective and potentiated cone signalling in darkness.

Introduction

The photoresponses in rod and cone photoreceptor cells are shaped by two opposing mechanisms: amplification and subsequent shut-off (Fu & Yau, 2007; Gulati & Palczewski, 2023; Kawamura & Tachibanaki, 2022; Lamb, 2022). All activated phototransduction proteins need to be deactivated in the shut-off process. Visual pigments are deactivated through phosphorylation of their C-terminal by G-protein coupled receptor kinase (GRK1) and capping by arrestin (Arr1) (Gurevich et al., 2011; Makino et al., 2003). Active GTP-bound transducin (G_t) is deactivated through GTP hydrolysis facilitated by the regulator of G-protein signalling 9 (RGS9) complex (Chen, 2015). The second messenger cGMP, which is degraded during activation, is resynthesized from GTP by guanylyl cyclase (GC) (Dizhoor & Peshenko, 2021). Importantly, GRK and GC activities are modulated by the intracellular

© 2026 The Author(s). *The Journal of Physiology* published by John Wiley & Sons Ltd on behalf of The Physiological Society.

14697793, 2026, 22, Downloaded from https://physoc.onlinelibrary.wiley.com/doi/10.1113/JP291252 by University Of California Irvine Science Library Serials, Wiley Online Library on [18/11/2026]. See the Terms and Conditions (https://onlinelibrary.wiley.com/terms-and-conditions) on Wiley Online Library for rules of use; OA articles are governed by the applicable Creative Commons License

Ca^{2+} concentration. The photoresponse is driven by the closure of some or all of the cyclic nucleotide-gated cation channels in the outer segments of photoreceptors, which suppresses the influx of Na^+ and Ca^{2+} (Yau & Nakatani, 1985). However, intracellular Ca^{2+} continues to be extruded by sodium–calcium potassium exchangers (NCKX) (Vinberg, Chen et al., 2018). The resulting reduction in intracellular Ca^{2+} facilitates its release from the calcium binding proteins recoverin (also known as S-modulin) (Kawamura & Tachibanaki, 2022) and GC activating proteins (GCAPs: GCAP1 and GCAP2 in mouse) (Dizhoor & Peshenko, 2021; Wen et al., 2014), leading to activation of GRK and GC, respectively. Together, the coordinated work of these shut-off proteins ensures the complete termination of the dim flash response within ∼1 s in a dark-adapted mouse rod (Chen, Burns et al., 1999; Chen et al., 2000; Mendez et al., 2001; Xu et al., 1997) and ∼200 ms in a cone (Ingram et al., 2019; Nikonov et al., 2006; Sakurai et al., 2011).

The function of each shut-off protein has been extensively studied using knockout mice (Chen, Burns et al., 1999; Chen et al., 2000; Mendez et al., 2001; Xu et al., 1997). For example, rods lacking arrestin ($Arr1^{-/-}$ also known as $Sag^{-/-}$) show ∼70 times longer photoresponses than wild-type rods based on their integration time (Fu et al., 2008; Xu et al., 1997). The absence of arrestin also delays the decay of photoactivated rhodopsin and the subsequent regeneration of rhodopsin in rods (Frederiksen et al., 2016). $Arr1^{-/-}$ rods also show outer segment shortening and degeneration phenotypes, representing a model for Oguchi disease. As another example, $Gcaps^{-/-}$ rods have 2.5 times longer photoresponses and 8-fold higher sensitivity compared to wild-type rods (Mendez et al., 2001). In contrast to $Arr1^{-/-}$ mice, $Gcaps^{-/-}$ mice retain normal rod morphology at least for the first 8 months of age.

In our previous study, we used highly sensitive $Gcaps^{-/-}$ rods to detect the small signals derived from unliganded apo-opsin (Sato et al., 2019). $Gcaps^{-/-}$ rods showed discrete membrane current events frequently in the presence of a small number of apo-opsins. Based on that study, we proposed that apo-opsin is in equilibrium between a predominantly inactive state and rare active state, a notion also supported by single-molecule imaging performed by another group (Maeda et al., 2014). The shape of the individual discrete events in our recordings was similar to the single photon response, suggesting that amplification and shut-off mechanisms between photoactivated Meta II rhodopsin and the active state of apo-opsin might be common. Thus, we hypothesized that, similarly to Meta II rhodopsin, the active apo-opsin is deactivated by GRK and arrestin.

Here, we generated mutant mice lacking both GCAPs and rod arrestin ($Gcaps^{-/-}Arr1^{-/-}$) or GCAPs and GRK ($Gcaps^{-/-}Grk1^{-/-}$) to study the action of those shut-off proteins on the active apo-opsin. However, membrane current recordings from single mutant rods were not possible due to a sticky substance, probably proteoglycans, in front of their outer segments (see Results for details). Instead, we characterized photoresponses of the $Gcaps^{-/-}Arr1^{-/-}$ retina using *ex vivo* electroretinography (ERG). Using parallel microspectrophotometric analysis, we also investigated the effect of *Gcaps* and *Arr1* deletion on the lifetime of photoactivated rhodopsin. While our attempts to obtain single-cell responses from these rods to study apo-opsin signalling were ultimately unsuccessful, we performed transretinal recordings which led us to examining how the saturation of rods might modulate the signalling of cone photoreceptors.

Materials and methods

Chemicals

dl-2-Amino-4-phosphonobutyric acid (DL-AP4) was obtained from Tocris Bioscience (Bristol, UK). Meclofenamic acid (MFA) sodium salt was obtained from ThermoFisher Scientific (Waltham, MA, USA). Other chemical reagents were obtained from Sigma-Aldrich (Saint Louis, MO, USA).

Animals

All experiments were performed in accordance with the NIH Guide for the Care and Use of Laboratory Animals and the Association for Research in Vision and Ophthalmology Statement for the Use of Animals in Ophthalmic and Vision Research and were approved by the Institutional Animal Care and Use Committee of UC Irvine and by the Institutional Animal Care and Use Committee of the University of California, Los Angeles. Mice, both male and female, were housed in a specific-pathogen-free facility with a 12:12 h light dark cycle, fed a standard laboratory chow diet and water *ad libitum*, and used at the age of 1–1.5 months. Wild-type C57Bl/6J mice were obtained from Jackson Laboratory (Bar Harbor, ME, USA).

Generation of mutant mice

$Gcaps^{-/-}$ and $Arr1^{-/-}$ mice (kind gift from Dr Jeannie Chen, University of Southern California, Los Angeles, CA, USA) were crossed to generate $Gcaps^{+/-}Arr1^{+/-}$ mice. They were then crossed to obtain $Gcaps^{-/-}Arr1^{+/-}$ mice. Finally, $Gcaps^{-/-}Arr1^{+/-}$ mice were crossed to obtain littermate $Gcaps^{-/-}$, $Gcaps^{-/-}Arr1^{+/-}$ and $Gcaps^{-/-}Arr1^{-/-}$ mice. Genotyping was done at Trans-

© 2026 The Author(s). *The Journal of Physiology* published by John Wiley & Sons Ltd on behalf of The Physiological Society.

14697793, 2026, 22, Downloaded from https://physoc.onlinelibrary.wiley.com/doi/10.1113/JP291252 by University Of California Irvine Science Library Serials, Wiley Online Library on [18/11/2026]. See the Terms and Conditions (https://onlinelibrary.wiley.com/terms-and-conditions) on Wiley Online Library for rules of use; OA articles are governed by the applicable Creative Commons License

netyx (Cordova, TN, USA). *Gnat1*$^{-/-}$ mice were kindly provided by Dr Janis Lem (Tufts University, Boston, MA, USA).

Histology analysis

Mice were killed by CO_2 inhalation and subsequent cervical dislocation. A burn mark was made on the dorsal side of the cornea using a cautery pen (AA25, Bovie Medical Corporation, Clearwater, FL, USA), to obtain sections through the dorsal and ventral retina. The eyeball was enucleated, placed in a histology cassette, and fixed immediately in Hartman fixative for 24 h at room temperature. The fixed eyeball was washed in 70% (v/v) ethanol once and stored in 70% (v/v) ethanol at 4°C. Paraffin embedding, sectioning, and haematoxylin and eosin-staining were performed in the Ocular Microanatomy Core of the Brunson Centre for Translational Vision Research in UC Irvine. Sections were imaged using an inverted microscope (BZ-X, Keyence, Osaka, Japan).

Ex vivo transretinal ERG

Ex vivo transretinal ERG was performed as described previously (Abbas et al., 2022; Vinberg & Kefalov, 2015; Vinberg et al., 2014). Briefly, mice were kept in darkness for more than 3 h, typically overnight, for complete dark adaptation of photoreceptor cells. Mice were killed by CO_2 inhalation and subsequent cervical dislocation. Eyes were enucleated, and the cornea and lens were removed using a pair of micro scissors and fine forceps under a stereomicroscope with an infrared illuminator and infrared scope. The retina from one eyecup was isolated immediately in Locke's solution [112.5 mM NaCl, 3.6 mM KCl, 2.4 mM $MgCl_2$, 1.2 mM $CaCl_2$, 10 mM HEPES, 20 mM $NaHCO_3$, 3 mM sodium succinate, 0.5 mM sodium glutamate, 0.02 mM EDTA, 10 mM glucose, 0.1% (v/v) MEM vitamin solution (100×) and 0.2% (v/v) MEM amino acids (50×) solution, pH 7.4 by bubbling with 95%O_2/5%CO_2] supplemented with 20 μM dl-AP4 to block postsynaptic components of the photoresponse and with 100 μM $BaCl_2$ to suppress the slow glial PIII component (Vinberg et al., 2014) and used for photovoltage recordings. The same supplemented solution was used for perfusion. The retina was placed in an *ex vivo* ERG adaptor (Ocuscience, Henderson, NV, USA), perfused with warm Locke's solution (1.2 mL min^{-1}, 37°C), and exposed to a 500 nm green flash stimulus delivered from a custom-made light-emitting diode (LED) system (Sato et al., 2020). Light intensity was calibrated with an optometer (350 Linear/Log optometer, UDT Instruments, San Diego, CA, USA). Trans-retinal voltage was amplified with a differential amplifier (DP-311A, Warner Instruments, Hamden, CT, USA), low pass filtered (eight-pole Bessel at 30 Hz; Model 3382, Krohn-Hite, Brockton, MA, USA) and imported to a computer through a digitizer (Digidata 1440A, Molecular Devices, San Jose, CA, USA). Data acquisition and analysis were done with pClamp10 (Molecular Devices).

When the recording protocol from the first retina was less than 1 h, the second eyecup from the mouse was placed in a 35 mm diameter Petri dish with 2 mL of perfusion solution and stored at room temperature (22°C) in a dark box supplied with a continuous flow of humidified 95% O_2/5% CO_2 gas. The second retina was then peeled off from the eyecup and used for recordings immediately after the first retina was finished.

For rod recordings from *Arr1*$^{-/-}$ and *Gcaps*$^{-/-}$*Arr1*$^{-/-}$ retinas, an infrared goggle (Swift, Nightfox, Bristol, UK) was used to minimize rhodopsin activation during euthanasia of mice and placement of the *ex vivo* ERG adaptor on the recording stage. [Correction added on 14 November 2026, after first online publication: This sentence has been updated.] For other recordings dim 660 nm red headlamp (D25LR, Sofirn, Shenzhen City, Guangdong, China) was used.

Intensity–response relationships were fitted with a Naka–Rushton hyperbolic function:

$$R = R_{\max} \cdot I^n / \left(I^n + {I_{1/2}}^n\right) \quad (1)$$

where $R_{\max}$ is the maximum response amplitude (μV), I is flash intensity (photons μm^{-2}), n is the Hill coefficient, and $I_{1/2}$ is the half-saturating flash intensity (photons μm^{-2})

For cone recordings from wild-type and *Gnat1*$^{-/-}$ retinas, the dorsal part of the retina was cut out and used for recordings to obtain responses from green-light-sensitive M-cones (Nikonov et al., 2006). The dorsal piece of the retina was placed in the *ex vivo* ERG adaptor and pre-conditioned for 15 min under 500 nm background light calibrated at 21,000 photons μm^{-2} s^{-1}. Rod saturation at this intensity was confirmed by separate single cell suction recordings and by measuring a shift of the photoresponse λ_{max} from 507 to 519 nm, which coincides with the different absorption peak wavelength of rhodopsin and M-cone pigment (see Results for details). Cone responses were obtained under the same background light with 50 ms 500 nm flashes.

Single cell suction recordings

Retinas were obtained as described for the *ex vivo* transretinal ERG method and cut into small pieces randomly with a razor blade. Retinal fragments were transferred into the perfusion chamber and imaged with an inverted microscope (IX51, Olympus, Tokyo, Japan) under infrared illumination. Tissues were perfused with warm (35–37°C) Locke's solution at 1.2 mL min^{-1}. A single rod outer

© 2026 The Author(s). *The Journal of Physiology* published by John Wiley & Sons Ltd on behalf of The Physiological Society.

14697793, 2026, 22, Downloaded from https://physoc.onlinelibrary.wiley.com/doi/10.1113/JP291252 by University Of California Irvine Science Library Serials, Wiley Online Library on [18/11/2026]. See the Terms and Conditions (https://onlinelibrary.wiley.com/terms-and-conditions) on Wiley Online Library for rules of use; OA articles are governed by the applicable Creative Commons License

segment was drawn in a glass micropipette and stimulated with 2 or 20 ms flashes. The stimulation light source was the same as in the *ex vivo* transretinal ERG. Membrane current signals were amplified (Axopatch 200B, Molecular Devices), low pass filtered (eight-pole Bessel at 30 Hz) and imported to a computer through a digitizer. Data acquisition and analysis were done with pClamp10. Other details are written and recorded in our previous video article (Wang & Kefalov, 2010).

Microspectrophotometry

Spectral absorbance measurements were made with a custom-built single-beam microspectrophotometer (MSP) (Frederiksen et al., 2016; Frederiksen et al., 2021; Nymark et al., 2012). A measurement beam of monochromatic light was generated by a xenon-arc light source coupled to a scanning monochromator (Cairn Research, Faversham, UK). The beam was polarized with a Glan-Thompson prism mounted on a rotating stage, allowing measurements of absorbance spectra with the polarization of the incident measuring beam either parallel to the plane of the intracellular discs of the rods (T polarization) or parallel to the long axis of the outer segment (L polarization). All measurements reported here were made with T polarization. The size of the measurement beam was set with an adjustable slit (field stop) in the optical path. This slit was brought into focus at the plane of the preparation with a condenser lens (Ultrafluar Kondenser, Carl Zeiss, Oberkochen, Germany), mounted on a piezo-electric driver (Physik Instrumente, Karlsruhe, Germany), and slaved to the monochromator to correct for chromatic aberration. The measuring beam was adjusted to be a rectangle of the dimensions 3 × 6 μm. Transmitted light was collected through a Nikon 60× water immersion objective lens and focused on a photomultiplier tube (Hamamatsu Photonics, Shizuoka, Japan). The signal was amplified and digitized by an NI-USB 6356 board that interfaced with a Dell Windows computer running a custom written LabVIEW 18 (National Instruments, Bethesda, MD, USA) acquisition software.

Eyes were enucleated in darkness by means of infrared image converters (ITT Industries, Stamford, CT, USA). The anterior portion of the eye was cut, and the lens and cornea were removed in darkness with a dissection microscope (Carl Zeiss) equipped with infrared image converters (ITT Industries) under near infrared illumination. Tissue was stored at 32°C in a light-tight container in Ames' medium supplemented with 1.9 g L^{-1} $NaHCO_3$ and equilibrated with 95% O_2/5% CO_2 at pH 7.4. The retina was isolated from the eyecup and the retinal pigment epithelium with fine tweezers. A retinal piece was gently flat mounted with forceps onto a quartz coverslip window in the bottom polyoxymethylene recording chamber with the photoreceptors facing upwards. A slice anchor was placed on top of the tissue to keep it stable throughout the experiment and the recording chamber was mounted on the motorized stage located in the beam path of the MSP. The retinal tissue was superfused at a rate of 4 mL min^{-1} with Ames' medium buffered with $NaHCO_3$ and equilibrated with 95% O_2/5% CO_2. Temperature was maintained at 35–37°C. Absorption spectra were measured from a region of the retina along its edge where rod outer segments could be seen protruding and perpendicular to the light beam. We recorded spectra over the wavelength range of 360–720 nm with 2 nm resolution. The absorbance spectrum was calculated according to Beer's Law:

$$\mathrm{OD} = \log_{10} \frac{I_i}{I_t} \tag{2}$$

where OD is the optical density, I_i is the light transmitted through a cell-free space adjacent to the outer segments and I_t is the light transmitted through the tissue. One assumption intrinsic to Equation (2) is that the beam is transmitted through an infinitely narrow slit at the centre of the long axis of the outer segment, so that the path length is equal to the outer segment diameter. Because we were recording from multiple cells and the slit was wider than a single outer segment, we had to compensate for a non-uniform path length. For a cylindrical outer segment of diameter d, and a slit width of w, we can calculate the corrected optical density $\mathrm{OD}_{\mathrm{corr}}$:

$$\mathrm{OD}_{\mathrm{corr}}\ (w, d) = \mathrm{OD}\frac{d}{\frac{2}{w}\left(\frac{d}{2}\right)^2\left[\arcsin\left(\frac{a}{d/2}\right) + \frac{a}{d/2}\sqrt{1-\left(\frac{a}{d/2}\right)^2}\right]} \tag{3a}$$

where:

$$a = \min\left(\frac{w}{2}, \frac{d}{2}\right) \tag{3b}$$

The MSP has a separate bleaching light path that is combined with the measurement beam through a pellicle. The bleaching light was produced by a 505 nm LED (Cairn Research). The LED produced a uniform illumination through a diaphragm field stop focused at the plane of the preparation. The intensity of the bleaching light was calibrated with a photodiode (Graseby Optronics) connected to a PDA200C photodiode amplifier (Thorlabs). The fraction of pigment bleach, F, was calculated using the bleaching equation:

$$F = 1 - e^{-IPt} \tag{4}$$

© 2026 The Author(s). *The Journal of Physiology* published by John Wiley & Sons Ltd on behalf of The Physiological Society.

14697793, 2026, 22, Downloaded from https://physoc.onlinelibrary.wiley.com/doi/10.1113/JP291252 by University Of California Irvine Science Library Serials, Wiley Online Library on [18/11/2026]. See the Terms and Conditions (https://onlinelibrary.wiley.com/terms-and-conditions) on Wiley Online Library for rules of use; OA articles are governed by the applicable Creative Commons License

where I is the light intensity in incident photons $\mu m^{-2}\ s^{-1}$, t is time in seconds and P is the photosensitivity for mouse rhodopsin of $5.7 \times 10^{-9}\ \mu m^2$ (Woodruff et al., 2004).

The photobleaching products meta II and meta III were extracted in the following way. First, a dark-adapted rhodopsin spectrum was recorded. This spectrum was baseline corrected by fitting a linear combination of an A1 nomogram (Govardovskii et al., 2000) and a polynomial (5th degree) representing the scattering of the beam (around the outer segments) by the non-absorptive tissue. This works because the unbleached rhodopsin spectrum of mouse rods is stereotypical and very well fit by the A1 nomogram. This baseline was saved and later subtracted from all the spectra, including those recorded after bleaching. Second, the retina was bleached by a 15 s step of 505 nm light (3.9×10^7 photons $\mu m^{-2} s^{-1}$) calculated to bleach > 90% of the visual pigment (Equation 4), and absorbance spectra were recorded immediately after the bleach ($t = 0$ min), and at defined time intervals thereafter. Each of these spectra were baseline corrected with the baseline obtained from the dark-adapted recording. The corrected spectra were fitted with a template for Meta II:

$$\text{MetaII}\ (\lambda) = A_{\text{II}}\ \varepsilon_{\text{II}} e^{\frac{-1}{2}\left(\frac{\lambda-378}{28}\right)^2} \quad (5)$$

where A_{II} is the peak amplitude of Meta II, normalized to rhodopsin, at 378 nm, ε_{II} is the extinction coefficient of Meta II relative to rhodopsin (1.16; Kolesnikov et al., 2003) and λ is wavelength. The Meta II template was subtracted from the spectra and the resulting Meta II-free spectra were fitted with a template for Meta III:

$$\text{MetaIII}\ (\lambda) = A_{\text{III}}\ \varepsilon_{\text{III}} \left[e^{\frac{-1}{2}\left(\frac{\lambda-472}{39.5}\right)^2} + 0.1 e^{\frac{-1}{2}\left(\frac{\lambda-450}{45}\right)^2} \right] \quad (6)$$

where A_{III} is the peak amplitude of Meta III, normalized to rhodopsin, at 472 nm, ε_{III} is the extinction coefficient of Meta III relative to rhodopsin (1.0; Kolesnikov et al., 2003) and λ is wavelength. Finally, the baseline corrected spectra were overlaid with a linear combination of eqns (5) and (6) to confirm the fits:

$$S\ (\lambda) = \text{MetaII}\ (\lambda) + \text{MetaIII}\ (\lambda) \quad (7)$$

Statistical analysis

For two-group comparisons, the statistical significance of difference between parameters was tested with a two-tailed unpaired Student's t test. For multiple comparison, data were analysed using one-way ANOVA followed by Tukey's honest significant difference (HSD) multiple comparison test unless otherwise stated in the text.

Results

Rod degeneration in *Gcaps*$^{-/-}$*Arr1*$^{-/-}$ retina

In *Arr1*$^{-/-}$ mouse retinas, progressive and light-dependent rod degeneration has been reported from 3.3 to 12 months of age (Chen, Simon et al., 1999), and a light-independent reduction of cone number (∼24%) has been reported in 2-month-old mice (Brown et al., 2010). To minimize the effects of photoreceptor degeneration, we used 1- to 1.5-month-old young adult mice. To evaluate the extent of early rod degeneration in *Gcaps*$^{-/-}$*Arr1*$^{-/-}$ mice, retinal morphology was assessed (Fig. 1). As control, we used age-matched *Gcaps*$^{-/-}$ mice, as they have been reported to retain normal retinal morphology up to 8 months of age (Mendez et al., 2001). Retinal sections revealed that *Arr1*$^{-/-}$ and *Gcaps*$^{-/-}$*Arr1*$^{-/-}$ retinas appear slightly thinner than control *Gcaps*$^{-/-}$ retinas (Fig. 1*A*). The degree of rod degeneration was evaluated from the thickness of the retinal outer nuclear layer (ONL) and photoreceptor inner and outer segment layer (IS-OS) (Fig. 1*B* and *C*). Compared to control *Gcaps*$^{-/-}$ retinas, *Arr1*$^{-/-}$ retinas showed 16% thinner ONL (mean of values obtained at 0.5, 0.75, 1.0, 1.25 and 1.5 mm distant from the optic nerve head, both dorsal and ventral sides were used) and 27% thinner IS-OS. In comparison, retinal sections from *Gcaps*$^{-/-}$*Arr1*$^{-/-}$ mice revealed 15% thinner ONL and 21% thinner IS-OS. Tukey's HSD test showed adjusted P-values of <0.05 for some data points (Tables A1 and A2), supporting the reduced thickness in *Arr1*$^{-/-}$ and *Gcaps*$^{-/-}$*Arr1*$^{-/-}$ retinas. We consider this partial rod degeneration phenotype in *Arr1*$^{-/-}$ and *Gcaps*$^{-/-}$*Arr1*$^{-/-}$ retinas in the interpretation of our subsequent electrophysiological analyses. Sections from *Gcaps*$^{-/-}$*Grk1*$^{-/-}$ retinas were not obtained because of our failure to obtain single-cell suction recordings from this strain (see below).

Unobtainable single-cell suction recording from the *Gcaps*$^{-/-}$*Arr1*$^{-/-}$ retina

We first attempted to record rod photoresponses from *Gcaps*$^{-/-}$*Arr1*$^{-/-}$ mice by a suction electrode. However, these attempts were hampered by semi-transparent sticky material covering the outer surface of the retina (Video S1). We found that the same phenomenology impaired our ability to record from the rods of *Gcaps*$^{-/-}$*Grk1*$^{-/-}$ retinas. In contrast, single rod outer segments from control *Gcaps*$^{-/-}$ or *Gcaps*$^{-/-}$*Arr1*$^{+/-}$ mouse retinas were easily drawn into the recording pipette. The rods from *Gcaps*$^{-/-}$ and *Gcaps*$^{-/-}$*Arr1*$^{+/-}$ mice produced almost identical photoresponses (Fig. A1), consistent with the same response waveforms reported in *Arr1*$^{+/+}$ and *Arr1*$^{+/-}$ rods (Xu et al., 1997).

© 2026 The Author(s). *The Journal of Physiology* published by John Wiley & Sons Ltd on behalf of The Physiological Society.

14697793, 2026, 22, Downloaded from https://physoc.onlinelibrary.wiley.com/doi/10.1113/JP291252 by University Of California Irvine Science Library Serials, Wiley Online Library on [18/11/2026]. See the Terms and Conditions (https://onlinelibrary.wiley.com/terms-and-conditions) on Wiley Online Library for rules of use; OA articles are governed by the applicable Creative Commons License

Cone responses from the *Gcaps*$^{-/-}$*Arr1*$^{-/-}$ retina in *ex vivo* ERG recordings

As an alternative to obtaining outer segment currents, we used transretinal *ex vivo* ERG recordings to measure the photovoltage in *Gcaps*$^{-/-}$*Arr1*$^{-/-}$ and *Gcaps*$^{-/-}$*Grk1*$^{-/-}$ retinas. Retinas were dissected from a dark-adapted mouse and placed on the *ex vivo* ERG adaptor under infrared illumination. The adaptor was then placed on the recording stage under dim 660 nm red light and kept in darkness for 15 min for stabilization. The photoreceptor a-wave photoresponse was isolated by using inhibitors which block signal propagation to downstream neurons and Müller cells (see Materials and methods for details). Control *Gcaps*$^{-/-}$ and *Gcaps*$^{-/-}$*Arr1*$^{+/-}$ retinas showed large and slow a-wave responses, which are typical in the rod-dominant mouse retina (Fig. 2*A* top left and middle and 2*B*). Unexpectedly, the *Gcaps*$^{-/-}$*Arr1*$^{-/-}$ retina showed cone-like fast and small a-wave responses (Fig. 2*A* top right and 2*B*). The estimated

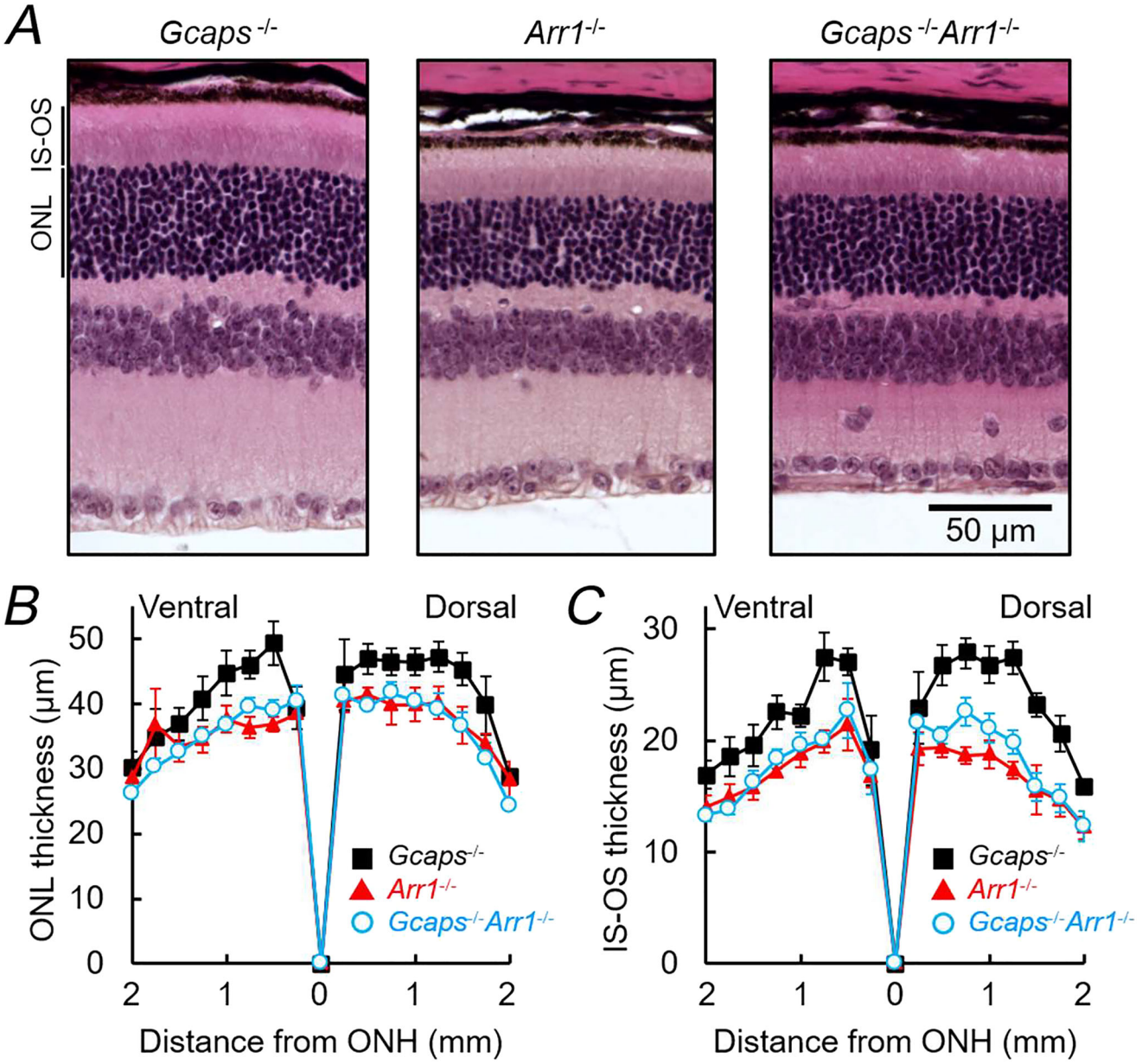


Figure 1. Rod degeneration in the *Gcaps*$^{-/-}$ *Arr1*$^{-/-}$ retina at 1 month of age
A, representative haematoxylin and eosin-stained retinal sections from *Gcaps*$^{-/-}$, *Arr1*$^{-/-}$ and *Gcaps*$^{-/-}$*Arr1*$^{-/-}$ retinas. Images are from the dorsal side of the retina at about 1 mm distant from the optic nerve head. *B* and *C*, plots of the ONL thickness (*B*) and IS-OS thickness (*C*) from vertical retinal sections. All plots are mean ± SEM (n = 4 or 5 mice).

© 2026 The Author(s). *The Journal of Physiology* published by John Wiley & Sons Ltd on behalf of The Physiological Society.

14697793, 2026, 22, Downloaded from https://physoc.onlinelibrary.wiley.com/doi/10.1113/JP291252 by University Of California Irvine Science Library Serials, Wiley Online Library on [18/11/2026]. See the Terms and Conditions (https://onlinelibrary.wiley.com/terms-and-conditions) on Wiley Online Library for rules of use; OA articles are governed by the applicable Creative Commons License

maximum response amplitude (R_{max}) of *Gcaps*$^{-/-}$*Arr1*$^{-/-}$ retinas (81 ± 25 μV, mean ± SD) was about 7.5-fold smaller than those in control *Gcaps*$^{-/-}$ (614 ± 103 μV) and *Gcaps*$^{-/-}$*Arr1*$^{+/-}$ (614 ± 127 μV) retinas (Fig. 2*B*, Table 1). In addition, the half-saturating light intensity ($I_{1/2}$) in *Gcaps*$^{-/-}$*Arr1*$^{-/-}$ retinas (620 ± 240 photons μm^{-2}) was about 25 times larger than in control *Gcaps*$^{-/-}$ (25 ± 5 photons μm^{-2}) and *Gcaps*$^{-/-}$*Arr1*$^{+/-}$ (27 ± 5 photons μm^{-2}) retinas (Fig. 2*B*, Table 1). Thus, the photosensitivity of *Gcaps*$^{-/-}$*Arr1*$^{-/-}$ retinas was reduced ∼25-fold compared to control retinas, consistent with the notion that even in darkness their responses were derived from cones and not from rods. To investigate further whether the responses from *Gcaps*$^{-/-}$*Arr1*$^{-/-}$ retinas are indeed generated by cones, we compared the spectral sensitivity of the three mutant strains. The data were fitted with the Govardovskii nomogram (Govardovskii et al., 2000) to estimate the peak wavelength λ_{max} for each

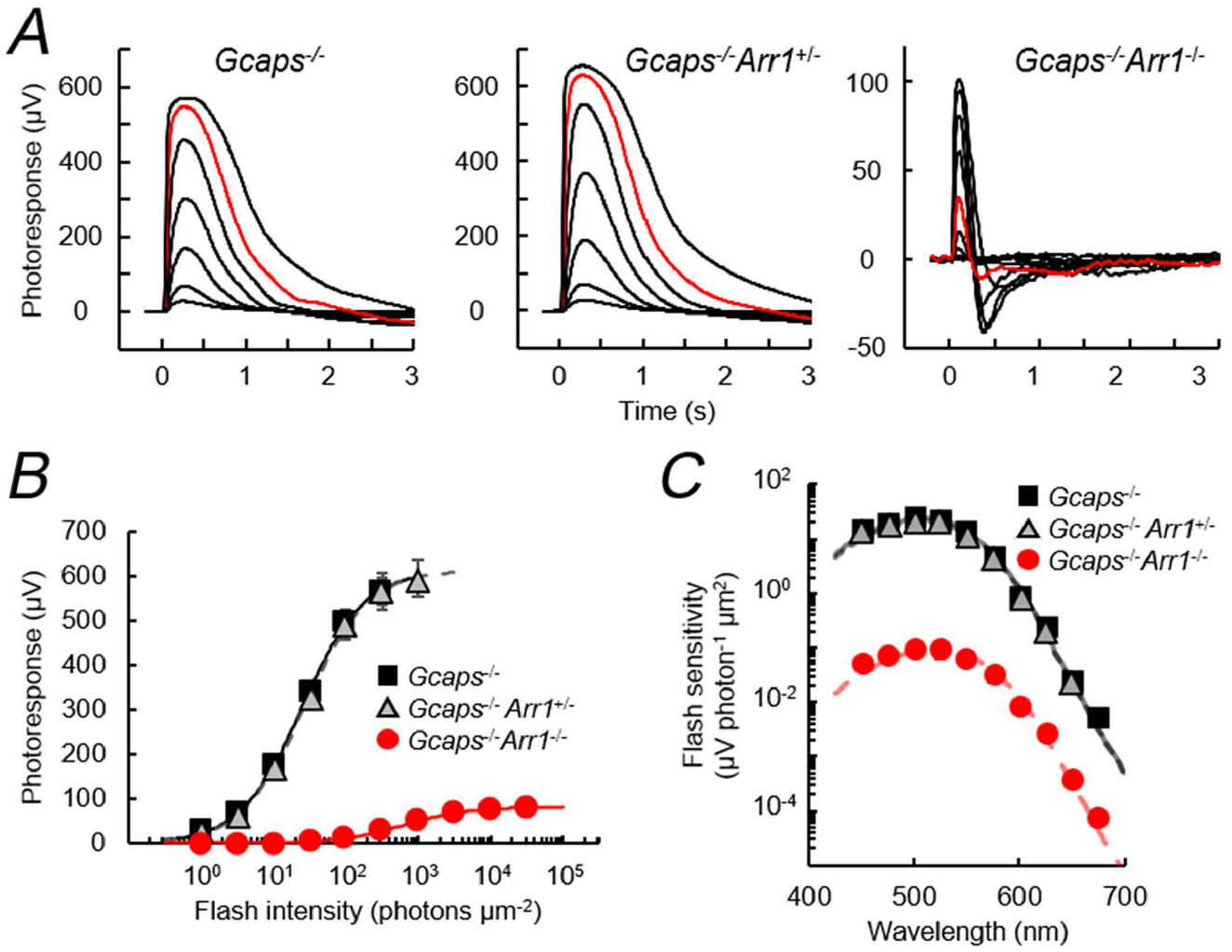


Figure 2. Modulation of photoresponses in GCAP-deficient retinas by the deletion of arrestin
A, representative flash response families from *Gcaps*$^{-/-}$, *Gcaps*$^{-/-}$*Arr1*$^{+/-}$ and *Gcaps*$^{-/-}$*Arr1*$^{-/-}$ mouse strains obtained by *ex vivo* ERG recordings from isolated retinas. The responses elicited from *Gcaps*$^{-/-}$ and *Gcaps*$^{-/-}$*Arr1*$^{+/-}$ retinas were rod-like, whereas the responses from *Gcaps*$^{-/-}$*Arr1*$^{-/-}$ retinas had cone-like characteristics. Flash intensity: 1–1000 photons μm^{-2} for *Gcaps*$^{-/-}$ and *Gcaps*$^{-/-}$*Arr1*$^{+/-}$ controls, and 1–32,000 photons μm^{-2} for *Gcaps*$^{-/-}$*Arr1*$^{-/-}$. Red traces show 320 photons μm^{-2} flash responses from each strain. *B*, intensity–response relationships for the light responses from *Gcaps*$^{-/-}$ and *Gcaps*$^{-/-}$*Arr1*$^{+/-}$ controls, and *Gcaps*$^{-/-}$*Arr1*$^{-/-}$ retinas. The responses from *Gcaps*$^{-/-}$*Arr1*$^{-/-}$ retinas were dramatically less sensitive than these from *Gcaps*$^{-/-}$ and *Gcaps*$^{-/-}$*Arr1*$^{+/-}$ retinas, consistent with their generation by cones *vs*. the rod-driven responses in control retinas. Plots are fitted with the Naka–Rushton hyperbolic function. *C*, spectral sensitivity of *Gcaps*$^{-/-}$ and *Gcaps*$^{-/-}$*Arr1*$^{+/-}$ controls, and *Gcaps*$^{-/-}$*Arr1*$^{-/-}$ retinas. The responses from *Gcaps*$^{-/-}$*Arr1*$^{-/-}$ retinas were red-shifted compared to those from *Gcaps*$^{-/-}$ and *Gcaps*$^{-/-}$*Arr1*$^{+/-}$ retinas, consistent with a switch from rhodopsin to M-cone pigment activation. Plots are fitted with the Govardovskii nomogram. All plots are mean ± SEM (n = 9 or 10 retinas). [Correction added on 14 November 2026, after first online publication: The figure legend has been modified.]

© 2026 The Author(s). *The Journal of Physiology* published by John Wiley & Sons Ltd on behalf of The Physiological Society.

14697793, 2026, 22, Downloaded from https://physoc.onlinelibrary.wiley.com/doi/10.1113/JP291252 by University Of California Irvine Science Library Serials, Wiley Online Library on [18/11/2026]. See the Terms and Conditions (https://onlinelibrary.wiley.com/terms-and-conditions) on Wiley Online Library for rules of use; OA articles are governed by the applicable Creative Commons License

Table 1. Flash response parameters

	R_{max} (μV)	$I_{1/2}$ (photons μm^{-2})	S_f (μV photon^{-1} μm^2)	Fractional S_f (photon^{-1} μm^2)	λ_{max} (nm)	*n*
Gcaps$^{-/-}$	614 ± 103	25 ± 5	18 ± 4	0.030 ± 0.005	508 ± 1	10 retinas
Gcaps$^{-/-}$ *Arr1*$^{+/-}$	614 ± 127 (1.000)	27 ± 5 (1.000)	17 ± 4 (0.846)	0.028 ± 0.003 (0.718)	508 ± 1 (0.779)	9 retinas
Gcaps$^{-/-}$ *Arr1*$^{-/-}$	81 ± 25 (< 0.001)	620 ± 240 (<0.001)	0.12 ± 0.06 (< 0.001)	0.0014 ± 0.0006 (< 0.001)	520 ± 2 (< 0.001)	9 retinas
Arr1$^{-/-}$[a]	328 ± 93 (< 0.001)	191 ± 104 (0.026)	1.5 ± 0.9 (< 0.001)	0.0047 ± 0.0025 (< 0.001)	NA	9 retinas
Gcaps$^{-/-}$ *Arr1*$^{-/-}$[a]	359 ± 77 (< 0.001)	27 ± 11 (1.000)	12 ± 4 (0.001)	0.034 ± 0.005 (0.113)	NA	8 retinas

Note: mean ± SD. Values in parentheses are *P* values from the Tukey's HSD test compared to *Gcaps*$^{-/-}$.
Abbreviation: NA; not analysed.
[a]Retinas were handled exclusively under infrared light to avoid exposure to the dim red light used in our normal procedure and to obtain selectively rod-driven responses.

strain. The spectral sensitivity of the *Gcaps*$^{-/-}$*Arr1*$^{-/-}$ retina peaked at 520 ± 2 nm (Fig. 2*C*, Table 1), which was 12 nm longer than that of control *Gcaps*$^{-/-}$ rods (508 ± 1 nm) and consistent with the difference in λ_{max} of mouse rhodopsin (500 nm; Fan et al., 2003) and M-cone pigment (508 nm; Sun et al., 1997). Together, these results demonstrate that photoresponses from the *Gcaps*$^{-/-}$*Arr1*$^{-/-}$ retina lacked a rod component and instead were generated by their cones. We noted that the amplitudes of these cone-driven responses in *Gcaps*$^{-/-}$*Arr1*$^{-/-}$ retina were somewhat larger than those previously obtained by us from *Gcaps*-deficient retinas (Sakurai et al., 2011; see fig. 4) or from control retinas (Vinberg et al., 2017; see fig. 9), both with rods lacking signalling due to the deletion of *Gnat1*. However, these recordings were done with different experimental tools, which might have contributed to any apparent differences. This prompted us to compare directly the cone responses from retinas with and without rod signalling as detailed in the 'Modulation of cone signals by rods' section below as a way of investigating how rod saturation could modulate the responses of cones.

The λ_{max} values for rods (508 nm) and cones (520 nm) in our analysis are 8–12 nm longer than the reported absorption maxima of rhodopsin (500 nm) and mouse M-cone pigment (508 nm). We suspected that this could be due to red-biased transmittance of light in our acrylic *ex vivo* ERG adaptor. However, direct measurements of the transmission through the adaptor cover showed only a slight bias in the range of 450–675 nm (Fig. A2). Notably, a similar albeit smaller red-shift was observed in our single-cell suction analysis from *Gcaps*$^{-/-}$ rods (504 ± 3 nm, mean ± SD, $n = 10$ rods). Although we have not identified the cause of this difference, we believe that it originates in the optical path shared between the *ex vivo* ERG and single-cell suction recordings.

We also tried to obtain *ex vivo* ERG recordings from *Gcaps*$^{-/-}$*Grk1*$^{-/-}$ retinas. However, we could not detect photoresponses in any of the six retinas that were tried (Fig. A3), prompting us to abandon this experiment and any further analysis of this strain.

Rod responses from the *Gcaps*$^{-/-}$*Arr1*$^{-/-}$ retina in *ex vivo* transretinal ERG recordings

As shown above, rod responses were not initially obtained from the *Gcaps*$^{-/-}$*Arr1*$^{-/-}$ retina in our *ex vivo* transretinal ERG recording attempts (Fig. 2). However, rod morphology appeared preserved in the age-matched *Gcaps*$^{-/-}$*Arr1*$^{-/-}$ retinas (Fig. 1), suggesting that rods must still be functional. Considering the slow photoresponse in *Gcaps*$^{-/-}$ rods (2.5 times longer integration time compared to wild-type controls; Mendez et al., 2001) and the extremely prolonged photoresponse in *Arr1*$^{-/-}$ rods (∼70 times; Fu et al., 2008; Xu et al., 1997), we hypothesized that *Gcaps*$^{-/-}$*Arr1*$^{-/-}$ rods might have remained in saturation after exposure to the dim 660 nm red light used for placing the *ex vivo* ERG adaptor on the microscope stage. To test this hypothesis, we extended the stabilization time for the retina from 15 min to >90 min, and dim flash responses were monitored every 5 min. Under these conditions we eventually detected a-waves driven by rod activity after ∼30 min of recording, which gradually recovered their amplitude until ∼90 min (Fig. 3*A* and *B*). To further confirm the initial rod saturation hypothesis, we used infrared light (850 nm) instead of 660 nm red light when setting up the recording chamber. Under these conditions, rod responses could be obtained immediately (Fig. 3*C* and *D*). We conclude that *Gcaps*$^{-/-}$*Arr1*$^{-/-}$ rods are functional but susceptible to saturation for extended periods of time by even a brief exposure to dim 660 nm red light.

Next, we characterized the flash responses of *Gcaps*$^{-/-}$*Arr1*$^{-/-}$ rods. As expected, *Gcaps*$^{-/-}$*Arr1*$^{-/-}$ rods showed minute-scale long photoresponses to flash stimuli (Fig. 4*A*), even longer than the extremely slow

© 2026 The Author(s). *The Journal of Physiology* published by John Wiley & Sons Ltd on behalf of The Physiological Society.

14697793, 2026, 22, Downloaded from https://physoc.onlinelibrary.wiley.com/doi/10.1113/JP291252 by University Of California Irvine Science Library Serials, Wiley Online Library on [18/11/2026]. See the Terms and Conditions (https://onlinelibrary.wiley.com/terms-and-conditions) on Wiley Online Library for rules of use; OA articles are governed by the applicable Creative Commons License

Arr1$^{-/-}$ rod responses. Because of this very long recovery time between flashes, we collected responses only at three flash intensities for *Arr1*$^{-/-}$ and *Gcaps*$^{-/-}$*Arr1*$^{-/-}$ rods. The maximal response amplitude of *Gcaps*$^{-/-}$*Arr1*$^{-/-}$ and *Arr1*$^{-/-}$ rods was smaller than that of *Gcaps*$^{-/-}$ rods (Fig. 4*B*). The estimated R_{max} value of *Gcaps*$^{-/-}$*Arr1*$^{-/-}$ rods was 359 ± 77 μV (mean ± SD, Table 1), which was comparable to the value in *Arr1*$^{-/-}$ rods (328 ± 93 μV) but about 40% smaller than the R_{max} value of *Gcaps*$^{-/-}$ rods (614 ± 103 μV). This smaller response amplitude could be attributed to the combined 15% fewer rods, as estimated from the ONL thinning (Fig. 1*B*), and their 21%

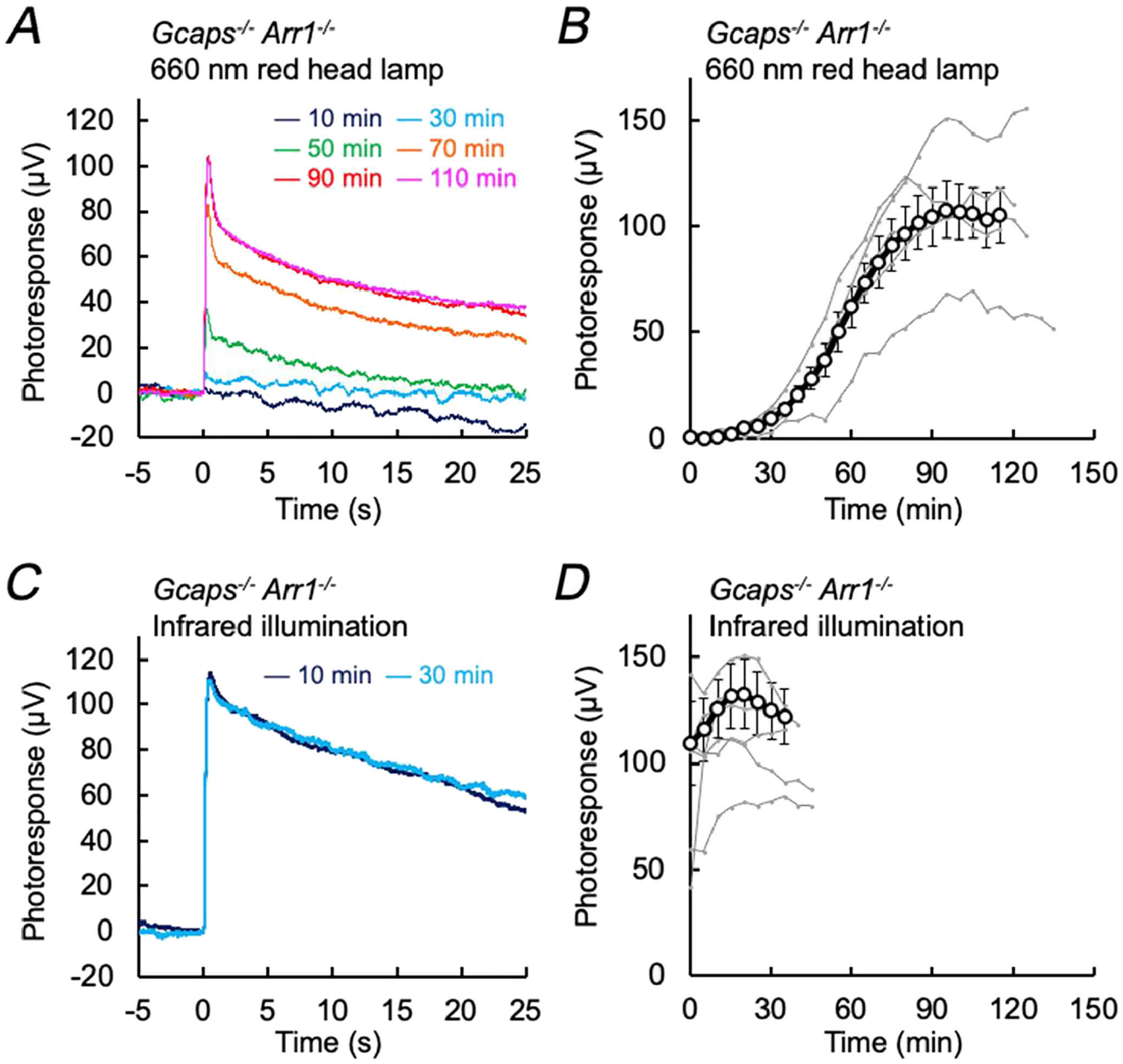


Figure 3. Initial suppression followed by gradual recovery of rod responses of *Gcaps*$^{-/-}$*Arr1*$^{-/-}$ retinas after brief exposure to red light
A, *ex vivo* ERG responses to 10 photons μm^{-2} flash recorded from a *Gcaps*$^{-/-}$*Arr1*$^{-/-}$ retina placed in the recording system under dim 660 nm red light. Traces at different time points after brief exposure to red light are colour-coded. Note that the *x*-axis scale is ∼10 times longer than that in Fig. 2. *B*, rod response recovery over time after brief exposure to red light during the dissection. Time 0 is when the retina was placed in the recording system under red light and exposed to perfusion. Grey: records from individual retinas, black: average curve from five retinas. *C*, responses to 10 photons μm^{-2} flash recorded from the retina placed in the recording system under infrared light. *D*, plots of response amplitude shown as in *B*. Records from five retinas.

© 2026 The Author(s). *The Journal of Physiology* published by John Wiley & Sons Ltd on behalf of The Physiological Society.

14697793, 2026, 22, Downloaded from https://physoc.onlinelibrary.wiley.com/doi/10.1113/JP291252 by University Of California Irvine Science Library Serials, Wiley Online Library on [18/11/2026]. See the Terms and Conditions (https://onlinelibrary.wiley.com/terms-and-conditions) on Wiley Online Library for rules of use; OA articles are governed by the applicable Creative Commons License

thinner IS-OS (Fig. 1*C*), probably due to the outer segment shortening as reported for *Arr1*$^{-/-}$ rods. The estimated $I_{1/2}$ of *Gcaps*$^{-/-}$*Arr1*$^{-/-}$ rods was 27 ± 11 photons μm^{-2} (Table 1), which was similar to *Gcaps*$^{-/-}$ rods (25 ± 5 photons μm^{-2}) and 7-fold smaller to that in *Arr1*$^{-/-}$ rods (191 ± 104 photons μm^{-2}). Thus, *Gcaps*$^{-/-}$*Arr1*$^{-/-}$ rods are 7-fold more sensitive than *Arr1*$^{-/-}$ rods, which is consistent with the 8-fold lower $I_{1/2}$ in *Gcaps*$^{-/-}$ rods compared to control wild-type rods (Mendez et al., 2001). Together, these results demonstrate that *Gcaps*$^{-/-}$*Arr1*$^{-/-}$ rods possess both the very slow photoresponse phenotype found in *Arr1*$^{-/-}$ rods and the high photosensitivity phenotype present in *Gcaps*$^{-/-}$ rods.

The extremely slow response kinetics of *Gcaps*$^{-/-}$*Arr1*$^{-/-}$ rods were analysed from dim flash responses (Fig. 4*C* and Table 2). Overall, *Gcaps*$^{-/-}$*Arr1*$^{-/-}$ rods showed about 100-fold slower response than *Gcaps*$^{-/-}$ rods (Fig. 4*C*), which is reflected in their two orders of magnitude longer integration time and recovery time constant (Table 2). As expected, *Arr1*$^{-/-}$ rods showed an initial rapid partial recovery, believed to be driven by partial deactivation of the visual pigment by rhodopsin kinase (Chen, Burns et al., 1999). However, this initial recovery was not observed in *Gcaps*$^{-/-}$ and *Gcaps*$^{-/-}$*Arr1*$^{-/-}$ rods, indicating that this step is likely to be controlled by the calcium feedback mechanism through GCAPs. The lack of this rapid recovery resulted in 2.5 times larger integration time in *Gcaps*$^{-/-}$*Arr1*$^{-/-}$ than in *Arr1*$^{-/-}$. The time to peak of *Gcaps*$^{-/-}$*Arr1*$^{-/-}$ rods was 481 ± 53 ms (mean ± SD), which is even longer than that of *Gcaps*$^{-/-}$ rods (293 ± 19 ms, $P = 1.47 \times 10^{-8}$, Student's *t* test), suggesting that the recovery in *Gcaps*$^{-/-}$ rods is accelerated by arrestin capping. The recovery time constant of *Gcaps*$^{-/-}$*Arr1*$^{-/-}$ (74,300 ± 16,000 ms) was larger than that of *Arr1*$^{-/-}$ (45,600 ± 25,900 ms, $P = 0.0211$), consistent with the

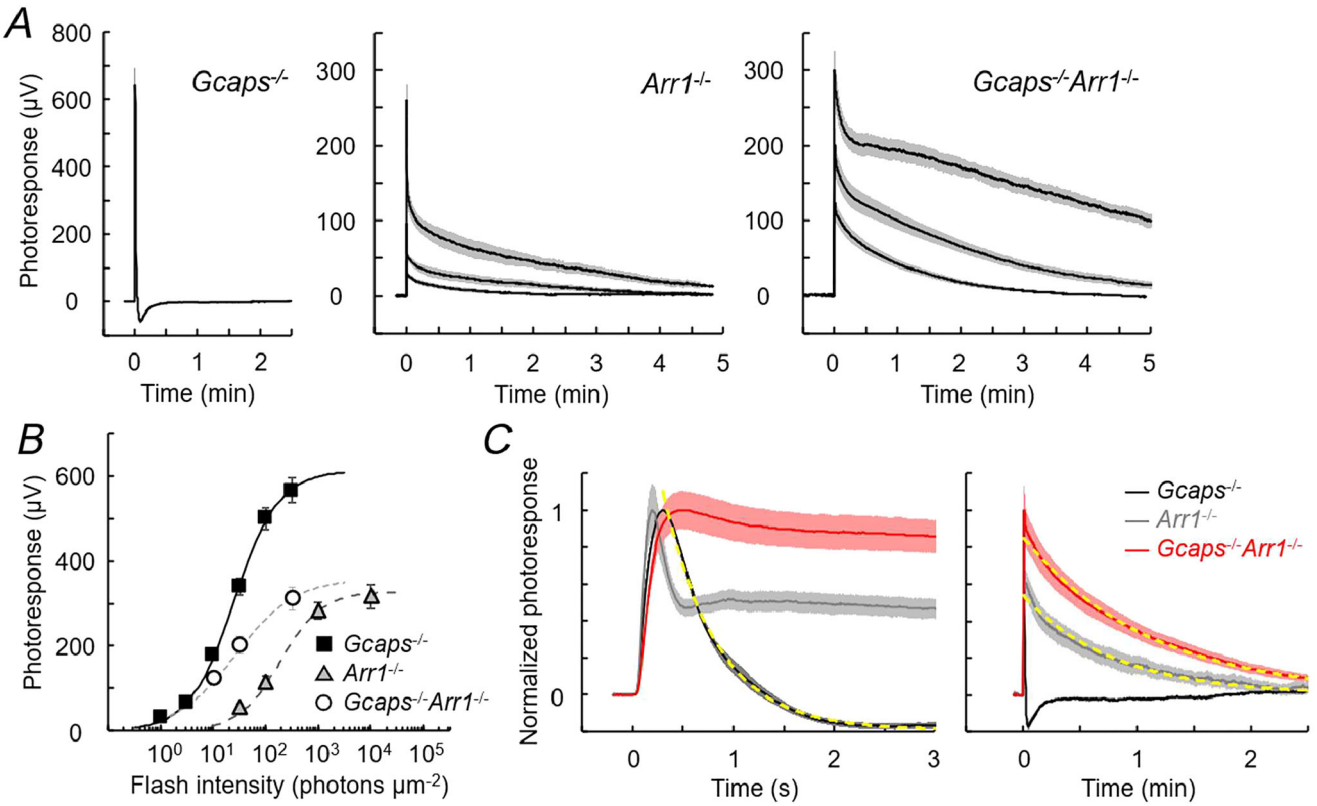


Figure 4. Modulation of photoresponses in GCAP-deficient rods by the deletion of arrestin
A, representative rod flash response families from *Gcaps*$^{-/-}$, *Arr1*$^{-/-}$ and *Gcaps*$^{-/-}$*Arr1*$^{-/-}$ retinas obtained by *ex vivo* ERG recordings. Flash intensity: 1000 photons μm^{-2} for *Gcaps*$^{-/-}$; 32, 100 and 1000 photons μm^{-2} for *Arr1*$^{-/-}$; 10, 32 and 320 photons μm^{-2} for *Gcaps*$^{-/-}$*Arr1*$^{-/-}$ rods. Mean ± SEM (n = 6 or 8 retinas). *B*, intensity–response relationships for the rod responses from *Gcaps*$^{-/-}$, *Arr1*$^{-/-}$ and *Gcaps*$^{-/-}$*Arr1*$^{-/-}$ retinas. Plots were fitted with the Naka–Rushton hyperbolic function. Plots for *Gcaps*$^{-/-}$ are replotted from Fig. 2. *C*, normalized rod dim flash responses for *Gcaps*$^{-/-}$, *Arr1*$^{-/-}$ and *Gcaps*$^{-/-}$*Arr1*$^{-/-}$ retinas. The left panel shows the first 3 s after the flash stimulation, and the right panel shows the same data in the longer 2.5 min scale. Mean ± SEM (n = 6–10 retinas). Fittings (yellow dashed curves) were made with a single exponential function $y = A^*\exp(-(t - t_o)/k) + C$ with following parameters, *Gcaps*$^{-/-}$: *A* 1.096, t_o 0.390 s, *k*: 0.520 s, *C*: −0.19; *Arr1*$^{-/-}$: *A* 0.532, t_o 0.515 s, *k*: 48.4 s, *C*: 0; *Gcaps*$^{-/-}$*Arr1*$^{-/-}$: *A* 0.847, t_o 0.515 s, *k*: 66.8 s, *C*: 0. [Correction added on 14 November 2026, after first online publication: The figure legend has been modified.]

© 2026 The Author(s). *The Journal of Physiology* published by John Wiley & Sons Ltd on behalf of The Physiological Society.

14697793, 2026, 22, Downloaded from https://physoc.onlinelibrary.wiley.com/doi/10.1113/JP291252 by University Of California Irvine Science Library Serials, Wiley Online Library on [18/11/2026]. See the Terms and Conditions (https://onlinelibrary.wiley.com/terms-and-conditions) on Wiley Online Library for rules of use; OA articles are governed by the applicable Creative Commons License

Table 2. Dim flash response kinetics parameters

	T_p (ms)	T_{int} (ms)	T_{rec} (ms)	*n*
Gcaps$^{-/-}$	293 ± 19	583 ± 88	503 ± 215	10 retinas
Arr1$^{-/-}$	190 ± 16	24,700 ± 16,100	45,600 ± 25,900[a]	9 retinas
Gcaps$^{-/-}$*Arr1*$^{-/-}$	481 ± 53	61,200 ± 23,200	74,300 ± 16,000	8 retinas

Note: mean ± SD.
[a]Two data points were excluded due to insufficient quality of curve fitting.

slower response recovery in *Gcaps*$^{-/-}$ rods compared with wild-type rods (Mendez et al., 2001). The dim flash response waveform in *Gcaps*$^{-/-}$*Arr1*$^{-/-}$ rods showed a simple exponential-like decay curve (Fig. 4*C* right), which led us to the analysis of the time course for the decay of Meta II rhodopsin (Frederiksen et al., 2016) as its possible rate-limiting process.

Decay of Meta II rhodopsin in *Gcaps*$^{-/-}$*Arr1*$^{-/-}$ rods in MSP measurement

We used MSP to investigate Meta II and Meta III lifetime in *Gcaps*$^{-/-}$*Arr1*$^{-/-}$ and *Gcaps*$^{-/-}$ rods following an extensive bleach (>90%, see Materials and methods for details). First, we recorded dark-adapted spectra from rods of both *Gcaps*$^{-/-}$ (Fig. 5*A*) and *Gcaps*$^{-/-}$*Arr1*$^{-/-}$ (Fig. 5*B*) mice. The *Gcaps*$^{-/-}$ dark-adapted recordings had an average optical density (OD) of 0.20 ± 0.039 (mean ± SD) and an average peak wavelength (λ_{max}) of 502 ± 2.0 nm. For *Gcaps*$^{-/-}$*Arr1*$^{-/-}$ the corresponding values were OD = 0.17 ± 0.060, consistent with the slight retinal thinning (Fig. 1), and λ_{max} = 501 ± 0.83 nm. We next bleached the retina and recorded the absorbance spectrum immediately thereafter. Absorbance spectra were recorded every minute for the first 10 min after bleach, then every 2 min until 20 min after bleach, and finally every 5 min until 60 min after bleach. A subset (0, 7 and 60 min) of these recordings are shown in Fig. 5*C* (*Gcaps*$^{-/-}$) and Fig. 5*D* (*Gcaps*$^{-/-}$*Arr1*$^{-/-}$). The traces were baseline corrected, normalized to fraction bleached rhodopsin and fit with a combination model of Meta II and Meta III (eqn 7). The traces labelled 0 min (red) in Fig. 5*C* and *D* show a large peak at 380 nm indicative of Meta II. A longer wavelength shoulder is also evident near 460–480 nm. This is probably indicative of the presence of a small amount of Meta I (peak at ∼460 nm) that is in fast equilibrium with Meta II (Vogel et al., 2004) as well as early formation of Meta III (peak at ∼472 nm). At 7 min (blue) the spectra were dominated by a 472 nm Meta III peak in both *Gcaps*$^{-/-}$ and *Gcaps*$^{-/-}$*Arr1*$^{-/-}$. This peak decayed completely in 60 min in *Gcaps*$^{-/-}$ (Fig. 5*C, green*) but persisted in *Gcaps*$^{-/-}$*Arr1*$^{-/-}$ (Fig. 5*D, green*).

From fits to recordings like those in Fig. 5*C* and *D*, we estimated the production and decay of Meta II (Fig. 5*E*) and Meta III (Fig. 5*F*) after a bleach. These data were fitted with bi-exponential functions (see Frederiksen et al., 2016; Nymark et al., 2012). Surprisingly, the decay time constants of Meta II were very similar between *Gcaps*$^{-/-}$ (τ_1 = 2.8 min; τ_2 = 7.6 min) and *Gcaps*$^{-/-}$*Arr1*$^{-/-}$ (τ_1 = 2.0 min; τ_2 = 7.2 min). In contrast, we observed a stark difference between the time course of Meta III in *Gcaps*$^{-/-}$ and *Gcaps*$^{-/-}$*Arr1*$^{-/-}$ (Fig. 5*F*). The time constants for production of Meta III were very similar (*Gcaps*$^{-/-}$: τ_1 = 2.8 min and *Gcaps*$^{-/-}$*Arr1*$^{-/-}$: τ_1 = 2.0 min), but the decay constant of Meta III was almost 3-fold slower in *Gcaps*$^{-/-}$*Arr1*$^{-/-}$ (*Gcaps*$^{-/-}$: τ_1 = 27 min and *Gcaps*$^{-/-}$*Arr1*$^{-/-}$: τ_1 = 78 min). Thus, the absence of arrestin resulted in a dramatic delay in the decay of Meta III to apo-opsin independently of the calcium feedback on cGMP synthesis.

Modulation of cone signals by rods

Surprisingly, the ERG responses from the *Gcaps*$^{-/-}$*Arr1*$^{-/-}$ retina in Fig. 2 contained only a cone component due to the prolonged rod saturation (see above). This is reminiscent of the *Gnat1*$^{-/-}$ retina which lacks the α subunit of rod transducin and, as a result, has only functional cones (Calvert et al., 2000). Although *Gnat1*$^{-/-}$ is a very convenient strain for studying mouse cones, its cone function is thought to be not entirely normal. For example, rods and cones are coupled at the synaptic terminal via connexin 36 gap junctions (Asteriti et al., 2014; Ishibashi et al., 2022), and thus rod input may affect cone development and function. This point is technically difficult to study with conventional single-cell electrophysiology methods in which tissue is sliced or chopped to partially disrupt the intercellular coupling network. To investigate this rod–cone interaction, we analysed semi-intact retinas by *ex vivo* ERG recordings. We first tried meclofenamic acid (MFA) a known gap junction blocker, on the *Gcaps*$^{-/-}$*Arr1*$^{-/-}$ retina. [Correction added on 14 November 2026, after first online publication: This sentence has been updated.] However, 100 μM MFA showed suppressive effects on both control *Gnat1*$^{-/-}$ and *Gcaps*$^{-/-}$*Arr1*$^{-/-}$ cone responses (Fig. A4), indicating that, at that concentration, MFA has off-target effects on cone phototransduction. Therefore,

© 2026 The Author(s). *The Journal of Physiology* published by John Wiley & Sons Ltd on behalf of The Physiological Society.

14697793, 2026, 22, Downloaded from https://physoc.onlinelibrary.wiley.com/doi/10.1113/JP291252 by University Of California Irvine Science Library Serials, Wiley Online Library on [18/11/2026]. See the Terms and Conditions (https://onlinelibrary.wiley.com/terms-and-conditions) on Wiley Online Library for rules of use; OA articles are governed by the applicable Creative Commons License

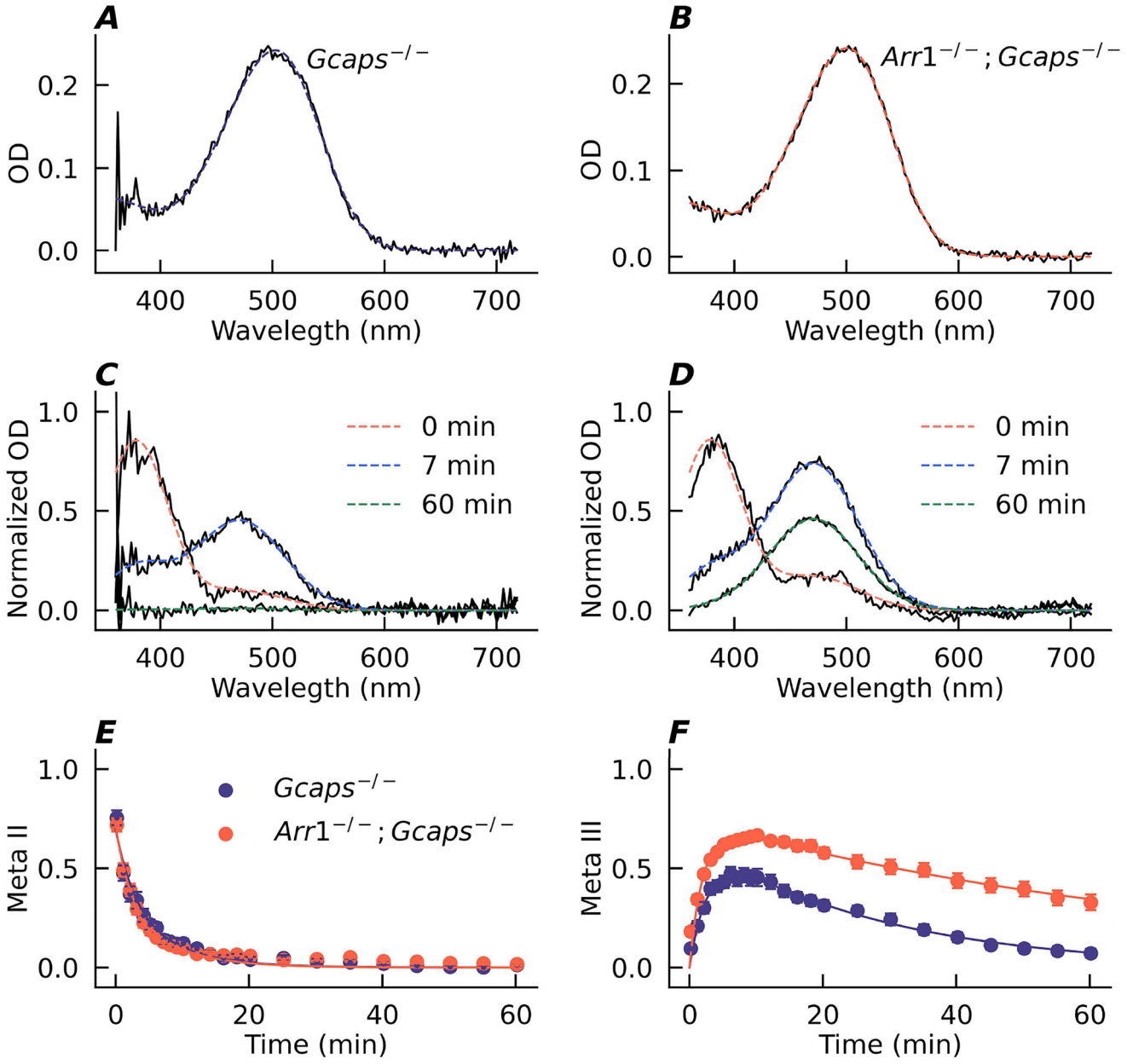


Figure 5. Microspectrophotometry recordings from *Gcaps*$^{-/-}$ and *Gcaps*$^{-/-}$ *Arr1*$^{-/-}$ mouse rods
A and *B*, dark-adapted absorbance spectra recorded from a representative *Gcaps*$^{-/-}$ (*A*) and *Gcaps*$^{-/-}$ *Arr1*$^{-/-}$ (*B*) retina. The spectra are baseline corrected and fitted with an A1 nomogram (Govardovskii et al. 2000). *C* and *D*, spectra recorded at time points after a > 90% bleach at 0 min (immediately, red), 7 min (blue) and 60 min (green) from a representative *Gcaps*$^{-/-}$ (*C*) and *Gcaps*$^{-/-}$*Arr1*$^{-/-}$ (*D*) retina. The spectra are baseline corrected, normalized to bleached rhodopsin and fitted with templates for Meta II and Meta III (eqn 7). *E*, time course of Meta II decay in *Gcaps*$^{-/-}$ (purple, $n = 11$) and *Gcaps*$^{-/-}$ *Arr1*$^{-/-}$ (red, $n = 11$) mouse rods. Data are fitted with a double exponential function with the time constants: $\tau_1 = 2.8$ min, $\tau_2 = 7.6$ min (*Gcaps*$^{-/-}$); and $\tau_1 = 2.0$ min, $\tau_2 = 7.2$ min (*Gcaps*$^{-/-}$*Arr1*$^{-/-}$). *F*, time course of Meta III production and decay in *Gcaps*$^{-/-}$ (purple, $n = 11$) and *Gcaps*$^{-/-}$ *Arr1*$^{-/-}$ (red, $n = 11$) mouse rods. Data are fitted with a double exponential function with the time constants: $\tau_1 = 2.8$ min, $\tau_2 = 27$ min (*Gcaps*$^{-/-}$); and $\tau_1 = 2.0$ min, $\tau_2 = 78$ min (*Gcaps*$^{-/-}$*Arr1*$^{-/-}$). Error bars in *E* and *F* are SEM.

© 2026 The Author(s). *The Journal of Physiology* published by John Wiley & Sons Ltd on behalf of The Physiological Society.

14697793, 2026, 22, Downloaded from https://physoc.onlinelibrary.wiley.com/doi/10.1113/JP291252 by University Of California Irvine Science Library Serials, Wiley Online Library on [18/11/2026]. See the Terms and Conditions (https://onlinelibrary.wiley.com/terms-and-conditions) on Wiley Online Library for rules of use; OA articles are governed by the applicable Creative Commons License

we compared *ex vivo* ERG responses from wild-type and *Gnat1*$^{-/-}$ M-cones. The dorsal piece of the retina, which is more enriched in M-cones than the ventral part (Nikonov et al., 2006), was used for this analysis. First, the responses were obtained in darkness (Fig. 6*A*). Large and slow rod responses were obtained from the wild-type retina. In contrast, small and fast cone responses were obtained from the *Gnat1*$^{-/-}$ retina. To isolate M-cone responses from the wild-type retina, the sample was then kept under rod-suppressing background light (500 nm 21,000 photons μm^{-2} s^{-1}) for 15 min (Fig. 6*B*). Under these conditions, the flash sensitivity of *Gnat1*$^{-/-}$ M-cones was reduced by 2.7-fold, from 0.025 ± 0.018 μV photon^{-1} μm^2 in darkness to 0.0093 ± 0.0034 μV photon^{-1} μm^2 in background light (mean ± SD, $n = 8$). This light-adapted M-cone sensitivity is expected to be still higher than the corresponding light-adapted rod sensitivity based on following estimation. The wild-type rod flash sensitivity in darkness was 2.5 ± 0.6 μV photon^{-1} μm^2 ($n = 10$). Based on a previous *ex vivo* ERG study from *Gnat2*$^{-/-}$ retinas in which only rods respond to light (Frederiksen et al., 2021), the rod desensitization after 15 min in the equivalent background light is between 1400- and 200,000-fold. Therefore, the estimated light-adapted rod sensitivity is 1.2×10^{-5} to 1.8×10^{-3} μV photon^{-1} μm^2, which is 5- to 775-fold lower than the sensitivity of light-adapted *Gnat1*$^{-/-}$ cones. Thus, photoresponses from light-adapted wild-type retinas would be dominated by M-cones, allowing direct comparison of cone responses in wild-type and *Gnat1*$^{-/-}$ retinas. Wild-type M-cone maximal response R_{max} was 107 ± 10 μV ($n = 10$), which was 1.5 times larger than that of *Gnat1*$^{-/-}$ M-cones (70 ± 17 μV, $n = 8$, $P = 2.70 \times 10^{-5}$, Student's *t* test). In addition, the half-saturating light intensity $I_{1/2}$ was 3,220 ± 750 photons μm^{-2} ($n = 10$) for wild-type M-cones, indicating 2.1 times higher sensitivity than *Gnat1*$^{-/-}$ M-cones with $I_{1/2}$ of 6,850 ± 1,380 photons μm^{-2} ($n = 8$, $P = 2.45 \times 10^{-6}$). Taken together,

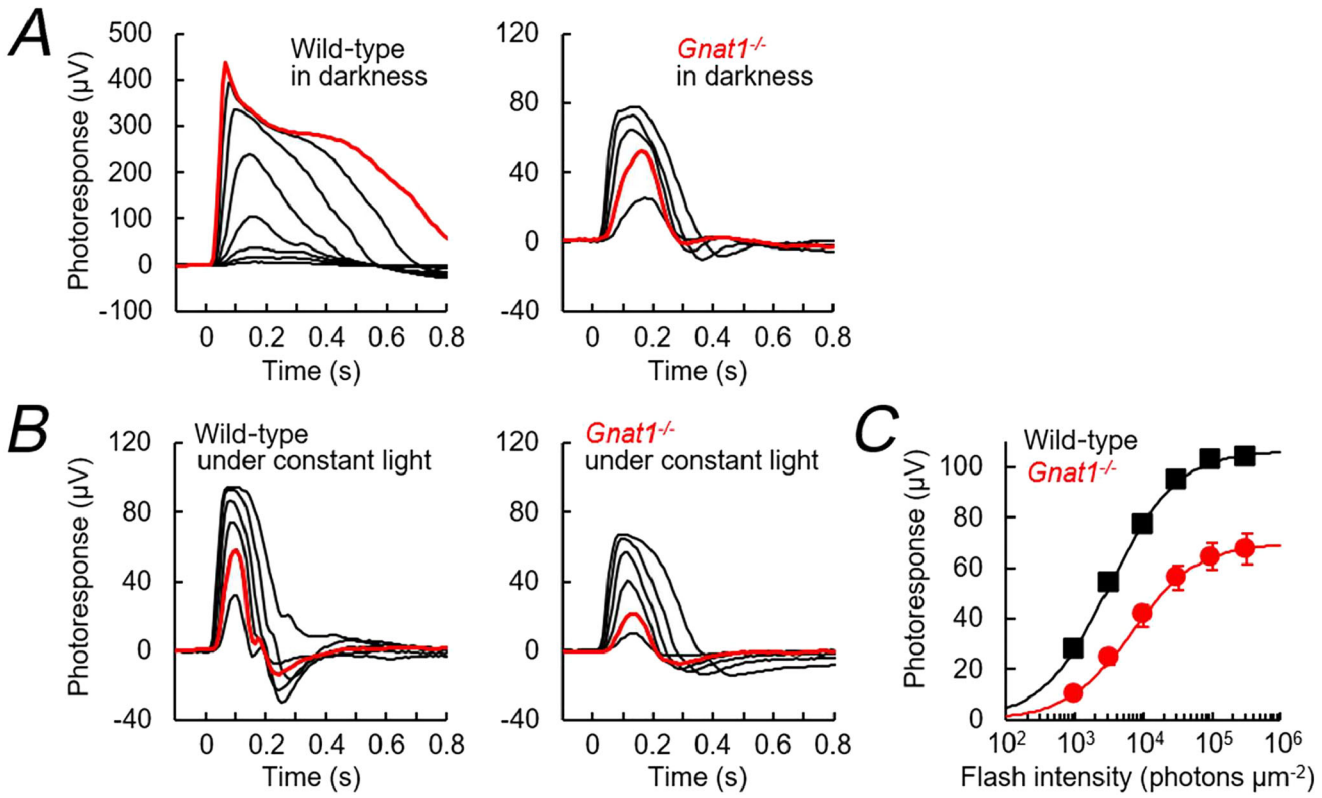


Figure 6. *Ex vivo* recordings from wild type and Gnat1$^{-/-}$ M-cones
A, *ex vivo* ERG responses from the dorsal piece of the retina in darkness. Flash intensity: 1–3200 photons μm^{-2} for wild-type and 1000–100,000 photons μm^{-2} for *Gnat1*$^{-/-}$ retinas. Red traces show 3200 photons μm^{-2} flash responses from each strain. *B*, cone *ex vivo* ERG responses under rod-saturating background light. The dorsal retina was exposed to 500 nm constant light calibrated at 21,000 photons μm^{-2} s^{-1} for 15 min prior to the flash response recordings. Flash intensity: 1000–320,000 photons μm^{-2}. Red traces show 3200 photons μm^{-2} flash responses. *C*, intensity response curves from wild-type and *Gnat1*$^{-/-}$ retinas under constant light. Data are shown as mean ± SEM, but some error bars are too small to be visible. n = 10 for wild-type and n = 8 for *Gnat1*$^{-/-}$ retinas. Plots are fitted with the Naka–Rushton hyperbolic function with the following parameters: wild-type: R_{max} 107 μV, $I_{1/2}$ 3220 photons μm^{-2}, n = 0.884; *Gnat1*$^{-/-}$: R_{max} 70 μV, $I_{1/2}$ 6850 photons μm^{-2}, n = 0.912.

© 2026 The Author(s). *The Journal of Physiology* published by John Wiley & Sons Ltd on behalf of The Physiological Society.

14697793, 2026, 22, Downloaded from https://physoc.onlinelibrary.wiley.com/doi/10.1113/JP291252 by University Of California Irvine Science Library Serials, Wiley Online Library on [18/11/2026]. See the Terms and Conditions (https://onlinelibrary.wiley.com/terms-and-conditions) on Wiley Online Library for rules of use; OA articles are governed by the applicable Creative Commons License

these results show that M-cone responses are larger and more sensitive when rods are saturated by background light. We conclude that cone photoresponses are potentiated by the input from rods.

Discussion

In the current study, we generated $Gcaps^{-/-}Arr1^{-/-}$ mice and characterized rod and cone photoresponses using *ex vivo* transretinal ERG recordings. Our results indicate that $Gcaps^{-/-}Arr1^{-/-}$ rods have extremely slow photoresponses, reminiscent of those observed by single-cell suction recordings from $Arr1^{-/-}$ rods (Fu et al., 2008; Xu et al., 1997). We find that the very slow rod responses in $Gcaps^{-/-}Arr1^{-/-}$ rods keep rod phototransduction in a saturated state for tens of minutes and enabled the recordings of cone ERG responses in darkness without the need to use persistent background light. This led us to investigate a possible rod–cone signalling interaction via gap junctions.

We were unable to perform single-cell suction recordings from $Gcaps^{-/-}Arr1^{-/-}$ rods because of the presence of a sticky substance covering the outer segment surface (Video S1). Rods and cones secrete interphotoreceptor matrix proteoglycan 1 (IMPG1, also known as sialoprotein associated with cones and rods, SPACR) around their outer segments (Salido & Ramamurthy, 2020), which binds viscous chondroitin sulphate and hyaluronan (Chandra et al., 1998; Zhao, Yoneda, Takeyama, Inoue et al., 2008; Zhao, Yoneda, Takeyama, Miyaishi et al., 2008). There may be overproduction of these interphotoreceptor matrix components in $Gcaps^{-/-}Arr1^{-/-}$ retinas. The sticky matter may be effectively removed by protease pretreatments, which is used in a cell dissociation method (Fadl et al., 2020).

We experienced the same issue with $Gcaps^{-/-}Grk1^{-/-}$ retinas. $Grk1^{-/-}$ rods show an extremely prolonged photoresponse (Chen, Burns et al., 1999) as seen in $Arr1^{-/-}$ rods. The sticky retina seems to be a general phenotype when the weakened calcium feedback in the $Gcaps^{-/-}$ rods is combined with a hyperactive rod phototransduction caused by additional mutations. A similar phenotype was observed in $Rho^{G90D/G90D}Gcaps^{-/-}$ retinas analysed in a recent study by us (in preparation), in which G90D rhodopsin has 175-fold higher spontaneous activation rate than the wild-type (Chai et al., 2024). Cone responses were not detected from $Gcaps^{-/-}Grk1^{-/-}$ retinas. This may be attributed to the lack of the cone-specific GRK subtype in the mouse retina: GRK1 is expressed in both mouse rods and cones (Chen et al., 2001). As a result deletion of *Grk1*, combined with the absence of GCAPs, would affect not only the shutoff of the rod responses but will also greatly delay the deactivation of the cone responses (Sakurai et al., 2011, 2015). In contrast, both rod and cone arrestin are expressed in mouse cones so that the deletion of rod arrestin alone is not sufficient to dramatically alter cone response deactivation (Nikonov et al., 2008).

In rod-dominant mouse retinas (97% rods 3% cones; Carter-Dawson & LaVail, 1979), cone ERG a-wave recordings are technically challenging unless using mutant mice such as $Gnat1^{-/-}$ which are deficient in their rod phototransduction (Vinberg et al., 2014). In the presence of functional rod phototransduction, a special illumination protocol such as rod-saturating background light (Vinberg, Peshenko et al., 2018) is applied to record cone responses on the top of the saturated rod signal. However, such protocols partially activate cone phototransduction before the test flash, which may affect the cone response properties. Indeed, we detected 2.1-fold desensitization of $Gnat1^{-/-}$ M-cones under rod-saturating background light. Additionally, the hyperpolarization of the rod network may influence the membrane potential of cones to subsequent light exposure. The $Gcaps^{-/-}Arr1^{-/-}$ retinas represent a unique case in which rod phototransduction is still functional but remains saturated for tens of minutes in complete darkness after a brief exposure to dim red light. We used this feature to obtain dark-adapted cone ERG responses without the need to ablate *Gnat1* and rod phototransduction. Importantly, $Gcaps^{-/-}Arr1^{-/-}$ cone photoresponses recover within a second, in contrast to the corresponding minutes-long rod responses. This is probably because mouse cones additionally express cone arrestin (also known as Arrestin-C or Arrestin-3, encoded by the *Arr3* gene, but also referred to as *Arr4* in some previous studies for historical reasons). Furthermore, even in the absence of both arrestin subtypes, cone pigments are rapidly deactivated by spontaneous chromophore dissociation (Nikonov et al., 2008).

Our *ex vivo* ERG approach allows analysis from semi-intact retinas, which keep the intercellular gap junction coupling network. Using this advantage we compared cone responses in the presence (wild-type) and absence ($Gnat1^{-/-}$) of functional rod phototransduction under rod-suppressing background light. The larger cone responses we obtained in wild-type retinas suggest the enhancement of cone signals by the rod signalling intruding via the rod–cone gap junction. Such input was directly demonstrated by patch clamp recordings from the soma of a mouse cone, which increases the measured response amplitude by about 1.5-fold (Ingram et al., 2019). This rod input is eliminated in both $Gnat1^{-/-}$ retinas where rods are not affected by the background light, and in connexin 36 knockout retinas where cones are uncoupled from the rods. These results indicate that the hyperpolarization of rods is communicated to cones via the rod–cone gap junctions. However, the same study shows that background light activating 9300

© 2026 The Author(s). *The Journal of Physiology* published by John Wiley & Sons Ltd on behalf of The Physiological Society.

14697793, 2026, 22, Downloaded from https://physoc.onlinelibrary.wiley.com/doi/10.1113/JP291252 by University Of California Irvine Science Library Serials, Wiley Online Library on [18/11/2026]. See the Terms and Conditions (https://onlinelibrary.wiley.com/terms-and-conditions) on Wiley Online Library for rules of use; OA articles are governed by the applicable Creative Commons License

rod pigment molecules per second ($R^*\ s^{-1}$) suppresses that additional rod component. The background light in our study (500 nm, 21,000 photons $\mu m^{-2}\ s^{-1}$) produces comparable rhodopsin activation (9900 $R^*\ s^{-1}$) based on the reported collecting area of a mouse rod (0.47 μm^2) (Sakurai et al., 2007). Therefore, the larger cone responses in the wild-type retina could not be explained by the addition of the rod component. There may be chronic effects of rod input on cone development and function. More investigation is needed on this point.

What is the rate-limiting mechanism in the extremely slow rod photoresponse recovery in the *Gcaps*$^{-/-}$*Arr1*$^{-/-}$ retina? Our MSP measurements revealed comparable decay of Meta II in *Gcaps*$^{-/-}$ and *Gcaps*$^{-/-}$*Arr1*$^{-/-}$ retinas but 3-fold slower decay of Meta III in the absence of arrestin. This observation is consistent with our previous work demonstrating that the lifetime of Meta III in *Arr1*$^{-/-}$ mouse rods is slower after a bleach (Frederiksen et al., 2016) and the *in vitro* findings by Sommer & Farrens (2006) that arrestin accelerates the decay of Meta III in a bovine rhodopsin preparation. The comparable Meta II lifetimes in *Gcaps*$^{-/-}$ and *Gcaps*$^{-/-}$*Arr1*$^{-/-}$ rods seem to be at odds with the slow rod photoresponse recovery in the *Gcaps*$^{-/-}$*Arr1*$^{-/-}$ retina. However, Meta II and Meta III are in equilibrium. It could be possible that a small amount of Meta II, which is below the detection limit of the MSP but enough to activate transducin, is consistently produced by this equilibrium. In this case, the prolonged Meta III in *Gcaps*$^{-/-}$*Arr1*$^{-/-}$ rods could at least partly explain their slow photoresponse recovery. This effect could be compounded by the disruption of the calcium feedback in the absence of GCAPs, and result in sustained rod signalling. In contrast, in the presence of arrestin, rhodopsin is rapidly inactivated, and as a result the decay of Meta II and Meta III will probably not modulate the rod response kinetics at all.

Overall, our results demonstrate that the simultaneous deletion of *Gcaps* and *Arr1* in mouse rods results in a dramatic delay in rod response recovery even after relatively dim light exposure so that rods remain saturated for minutes. This, in turn, allowed us to obtain selectively cone responses without the need for persistent background light.

Appendix

Table A1. Statistical data of ONL thickness used in Fig. 1*B*

		Gcaps$^{-/-}$				*Arr1*$^{-/-}$					*Gcaps*$^{-/-}$*Arr1*$^{-/-}$				
	[a]Position	Mean	*n*	SD	SEM	Mean	*n*	SD	SEM	[b]Adjusted *P*	Mean	*n*	SD	SEM	[b]Adjusted *P*
Ventral	2	30.2	4	4.97	2.48	28.6	5	4.27	1.91	0.810	26.3	5	1.83	0.819	0.309
	1.75	34.9	5	9.60	4.29	36.7	5	12.6	5.64	0.955	30.4	5	2.76	1.24	0.721
	1.5	36.9	5	5.65	2.53	33.4	5	5.21	2.33	0.517	32.6	5	3.26	1.46	0.376
	1.25	40.8	5	7.50	3.36	34.5	5	4.50	2.01	0.170	34.9	5	1.36	0.61	0.204
	1	44.8	5	7.63	3.41	37.7	5	4.65	2.08	0.135	36.8	5	2.83	1.27	0.0902
	0.75	46.1	5	4.87	2.18	36.4	5	3.65	1.63	**0.00532**	39.6	5	2.96	1.32	0.0537
	0.5	49.3	5	7.68	3.43	36.9	5	2.64	1.18	**0.00638**	39.0	5	3.72	1.66	**0.0202**
	0.25	39.4	5	7.30	3.26	38.5	5	1.85	0.828	0.964	40.6	5	5.24	2.34	0.931
Dorsal	0.25	44.5	5	12.3	5.5	40.4	5	3.65	1.63	0.671	41.1	5	1.80	0.807	0.761
	0.5	46.9	5	5.26	2.35	41.3	5	2.77	1.24	0.0759	39.7	5	2.11	0.944	**0.0222**
	0.75	46.6	5	4.62	2.06	39.8	5	6.66	2.98	0.141	41.6	5	3.76	1.68	0.323
	1	46.5	5	4.56	2.04	39.9	5	5.82	2.60	0.0881	40.5	5	2.18	0.976	0.124
	1.25	47.3	5	5.25	2.35	40.2	5	5.62	2.51	0.132	39.2	5	5.30	2.37	0.0825
	1.5	45.4	5	5.64	2.52	36.8	5	6.50	2.91	0.0830	36.5	5	4.95	2.21	0.0743
	1.75	39.8	5	10.1	4.53	33.7	5	3.94	1.76	**0.0388**	31.7	5	5.30	2.37	0.200
	2	28.7	4	2.12	1.06	28.4	5	5.96	2.67	0.994	24.3	4	2.83	1.41	0.345

[a] Position indicates distance from the optic nerve head.
[b] Adjusted *P* values were obtained by Tukey's HSD test for comparisons with *Gcaps*$^{-/-}$. Values less than 0.05 are highlighted in bold, and *n* indicates the number of mice.

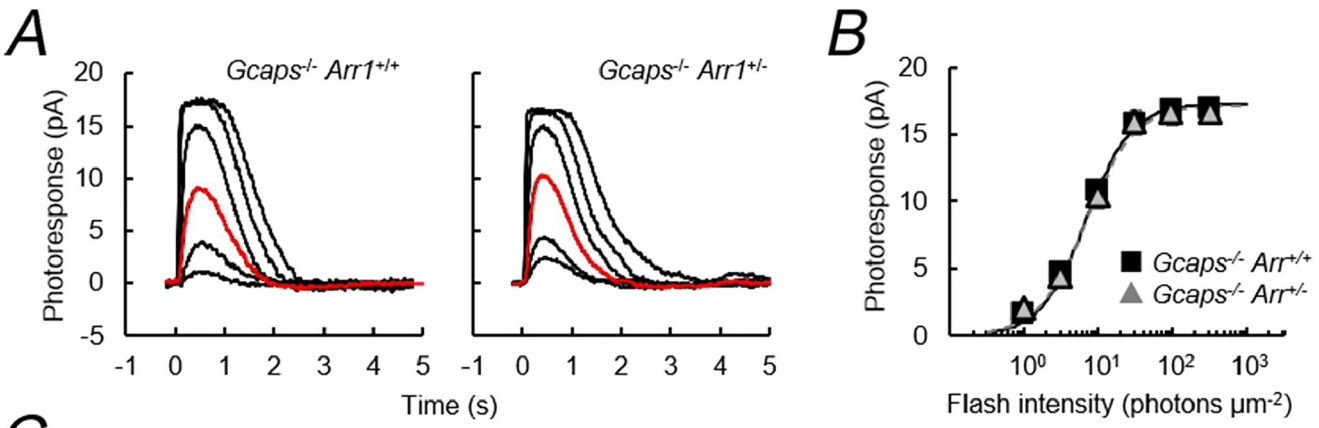
© 2026 The Author(s). *The Journal of Physiology* published by John Wiley & Sons Ltd on behalf of The Physiological Society.

14697793, 2026, 22, Downloaded from https://physoc.onlinelibrary.wiley.com/doi/10.1113/JP291252 by University Of California Irvine Science Library Serials, Wiley Online Library on [18/11/2026]. See the Terms and Conditions (https://onlinelibrary.wiley.com/terms-and-conditions) on Wiley Online Library for rules of use; OA articles are governed by the applicable Creative Commons License

Table A2. Statistical data of IS-OS thickness used in Fig. 1C.

		Gcaps$^{-/-}$				*Arr1*$^{-/-}$					*Gcaps*$^{-/-}$*Arr1*$^{-/-}$				
	[a]Position	Mean	*n*	SD	SEM	Mean	*n*	SD	SEM	[b]Adjusted *P*	Mean	*n*	SD	SEM	[b]Adjusted *P*
Ventral	2	16.9	4	2.61	1.30	14.0	5	2.35	1.05	0.133	13.3	5	1.05	0.47	0.0554
	1.75	18.6	5	3.97	1.77	14.9	5	2.60	1.15	0.143	13.9	5	1.21	0.54	0.0532
	1.5	19.5	5	4.16	1.86	15.8	5	2.51	1.12	0.177	16.3	5	2.21	0.99	0.253
	1.25	22.5	5	3.31	1.48	17.3	5	1.48	0.66	**0.011**	18.4	5	1.93	0.86	**0.0401**
	1	22.2	5	2.27	1.02	18.8	5	2.84	1.27	0.141	19.5	5	2.71	1.21	0.257
	0.75	27.5	5	4.79	2.14	19.9	5	2.33	1.04	**0.00568**	20.1	5	0.50	0.22	**0.00663**
	0.5	27.0	5	2.71	1.21	21.4	5	5.15	2.30	0.174	22.7	5	5.52	2.47	0.331
	0.25	19.1	5	6.98	3.12	16.8	5	2.19	0.98	0.750	17.4	5	4.89	2.19	0.861
Dorsal	0.25	22.9	5	7.20	3.20	19.3	5	3.18	1.42	0.458	21.5	5	2.00	0.90	0.883
	0.5	26.7	5	4.00	1.79	19.4	5	2.07	0.93	**0.00353**	20.5	5	1.77	0.79	**0.0102**
	0.75	27.8	5	3.08	1.38	18.6	5	1.76	0.79	**0.00033**	22.6	5	2.82	1.26	**0.0202**
	1	26.8	5	3.71	1.66	18.7	5	2.88	1.29	**0.00494**	21.1	5	3.01	1.35	**0.0400**
	1.25	27.4	5	3.29	1.47	17.3	5	1.64	0.73	**0.000105**	19.9	5	2.38	1.06	**0.00133**
	1.5	23.2	5	2.42	1.08	15.6	5	5.00	2.23	0.0141	15.8	5	2.72	1.22	**0.0175**
	1.75	20.6	5	3.60	1.60	14.6	5	3.22	1.44	0.0313	14.8	5	2.84	1.27	**0.0383**
	2	15.8	4	1.35	0.68	12.2	5	2.17	0.97	0.0660	12.3	4	2.67	1.33	0.0970

[a]Position indicates distance from the optic nerve head.
[b]Adjusted *P* values were obtained by Tukey's HSD test for comparisons with *Gcaps*$^{-/-}$. Values less than 0.05 are highlighted in bold, and *n* indicates the number of mice.



C

	R_{max} (pA)	$I_{1/2}$ (photon μm^{-2})	S_f (pA photon^{-1} μm^2)	*n*
Gcaps$^{-/-}$ *Arr*$^{+/+}$	17.3 ± 4.8	6.8 ± 1.9	1.4 ± 0.6	44 rods
Gcaps$^{-/-}$ *Arr*$^{+/-}$	17.2 ± 1.7	6.9 ± 1.3	1.5 ± 0.5	5 rods

Mean ± SD.

Figure A1. Rod flash response analysis
A, representative flash response families of a rod by the single-cell suction method. Flash: 500 nm, 1–320 photons μm^{-2}. Red traces show responses to 10 photons μm^{-2}. *B*, averaged intensity–response curves. Plots were fitted with the Naka–Rushton hyperbolic function. Error bars represent SEM, but they are too small to be visible. *C*, parameters obtained from *B*. R_{max}: estimated maximum response amplitude, $I_{1/2}$: half-saturating flash intensity, S_f: flash sensitivity.

© 2026 The Author(s). *The Journal of Physiology* published by John Wiley & Sons Ltd on behalf of The Physiological Society.

14697793, 2026, 22, Downloaded from https://physoc.onlinelibrary.wiley.com/doi/10.1113/JP291252 by University Of California Irvine Science Library Serials, Wiley Online Library on [18/11/2026]. See the Terms and Conditions (https://onlinelibrary.wiley.com/terms-and-conditions) on Wiley Online Library for rules of use; OA articles are governed by the applicable Creative Commons License

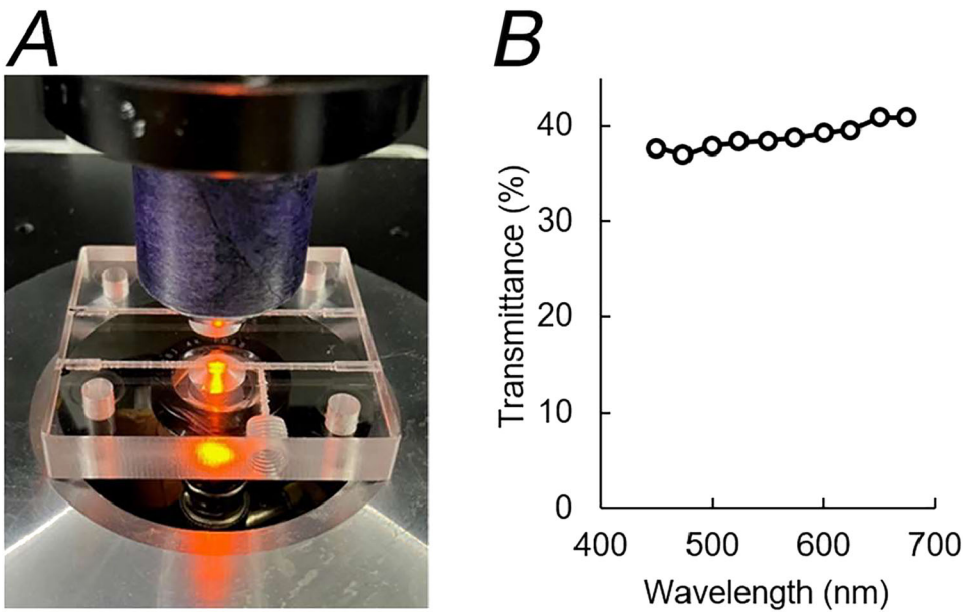


Figure A2. Measurement of the transmittance of the ex vivo ERG adaptor
A, The upper part of the transparent adaptor was placed on the sensor head of the power meter. The power was compared to the value obtained in the absence of the adaptor to obtain transmittance values. *B*, transmittance plot of the adaptor. [Correction added on 14 November 2026, after first online publication: The figure legend has been modified.]

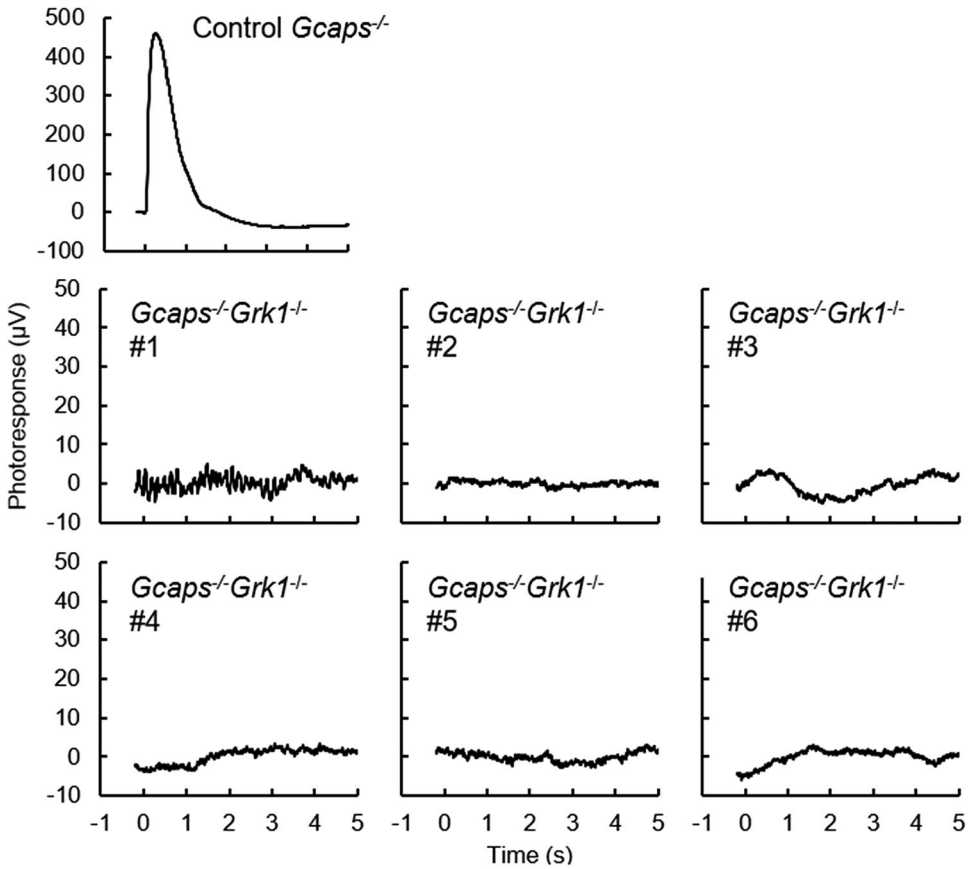
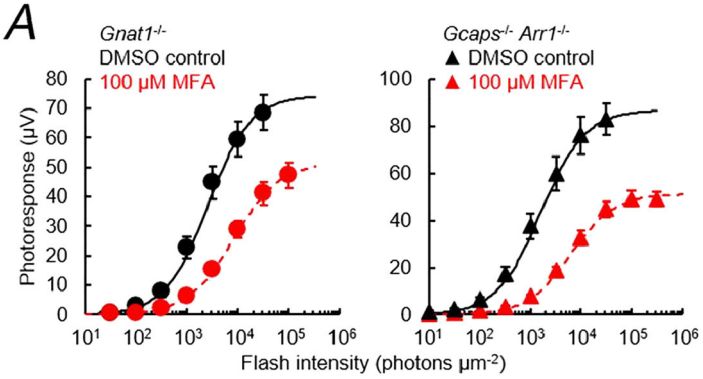


Figure A3. Voltage signals recorded with a 100 photons μm^{-2} 500 nm flash
The *y*-axis scale for *Gcaps*$^{-/-}$*Grk1*$^{-/-}$ panels are magnified ×10 to emphasize the lack of photoresponses.

© 2026 The Author(s). *The Journal of Physiology* published by John Wiley & Sons Ltd on behalf of The Physiological Society.

14697793, 2026, 22, Downloaded from https://physoc.onlinelibrary.wiley.com/doi/10.1113/JP291252 by University Of California Irvine Science Library Serials, Wiley Online Library on [18/11/2026]. See the Terms and Conditions (https://onlinelibrary.wiley.com/terms-and-conditions) on Wiley Online Library for rules of use; OA articles are governed by the applicable Creative Commons License

A



B

	R_{max} (μV)	$I_{1/2}$ (photon μm^{-2})	S_f (μV photon^{-1} μm^2)	Fractional S_f (photon^{-1} μm^2)	*n*
Gnat1$^{-/-}$, DMSO control	74 ± 16	2570 ± 1020	0.025 ± 0.018	0.00034 ± 0.00020	8 retinas
Gnat1$^{-/-}$, 100 μM MFA	52 ± 12	8200 ± 2560	0.0054 ± 0.0020	0.00011 ± 0.00005	8 retinas
Gcaps$^{-/-}$*Arr1*$^{-/-}$, DMSO control	87 ± 25	1620 ± 770	0.055 ± 0.033	0.00062 ± 0.00034	10 retinas
Gcaps$^{-/-}$*Arr1*$^{-/-}$, 100 μM MFA	51 ± 21	6240 ± 3020	0.0088 ± 0.0019	0.00017 ± 0.00004	10 retinas

Mean ± SD.

Figure A4. Effect of the gap junction blocker MFA on cone responses
A, intensity–response curves of control *Gnat1*$^{-/-}$ and *Gcaps*$^{-/-}$*Arr1*$^{-/-}$ cones with or without gap junction blocker MFA. Retinas were perfused with solution containing control vehicle DMSO or 100 μM MFA for 30 min prior to the recordings. Plots are mean ± SEM. *B*, parameters obtained from *A*.

© 2026 The Author(s). *The Journal of Physiology* published by John Wiley & Sons Ltd on behalf of The Physiological Society.

14697793, 2026, 22, Downloaded from https://physoc.onlinelibrary.wiley.com/doi/10.1113/JP291252 by University Of California Irvine Science Library Serials, Wiley Online Library on [18/11/2026]. See the Terms and Conditions (https://onlinelibrary.wiley.com/terms-and-conditions) on Wiley Online Library for rules of use; OA articles are governed by the applicable Creative Commons License

References

Abbas, F., Vinberg, F., & Becker, S. (2022). Optimizing the setup and conditions for ex vivo electroretinogram to study retina function in small and large eyes. *Journal of visualized experiments: JoVE*, **184**, e62763.

Asteriti, S., Gargini, C., & Cangiano, L. (2014). Mouse rods signal through gap junctions with cones. *eLife*, **3**, e01386.

Brown, B. M., Ramirez, T., Rife, L., & Craft, C. M. (2010). Visual arrestin 1 contributes to cone photoreceptor survival and light adaptation. *Investigative Ophthalmology & Visual Science*, **51**(5), 2372–2380.

Calvert, P. D., Krasnoperova, N. V., Lyubarsky, A. L., Isayama, T., Nicoló, M., Kosaras, B., Wong, G., Gannon, K. S., Margolskee, R. F., Sidman, R. L., Pugh, E. N., Makino, C. L., & Lem, J. (2000). Phototransduction in transgenic mice after targeted deletion of the rod transducin alpha -subunit. *Proceedings of the National Academy of Sciences of the United States of America*, **97**(25), 13913–13918.

Carter-Dawson, L. D., & Lavail, M. M. (1979). Rods and cones in the mouse retina. I. Structural analysis using light and electron microscopy. *Journal of Comparative Neurology*, **188**(2), 245–262.

Chai, Z., Ye, Y., Silverman, D., Rose, K., Madura, A., Reed, R. R., Chen, J., & Yau, K. W. (2024). Dark continuous noise from mutant G90D-rhodopsin predominantly underlies congenital stationary night blindness. *Proceedings of the National Academy of Sciences of the United States of America*, **121**(21), e2404763121.

Chandra, N., Brew, K., & Acharya, K. R. (1998). Structural evidence for the presence of a secondary calcium binding site in human alpha-lactalbumin. *Biochemistry*, **37**(14), 4767–4772.

Chen, C. K. (2015). RGS protein regulation of phototransduction. *Progress in Molecular Biology and Translational Science*, **133**, 31–45.

Chen, C. K., Burns, M. E., He, W., Wensel, T. G., Baylor, D. A., & Simon, M. I. (2000). Slowed recovery of rod photoresponse in mice lacking the GTPase accelerating protein RGS9-1. *Nature*, **403**(6769), 557–560.

Chen, C. K., Burns, M. E., Spencer, M., Niemi, G. A., Chen, J., Hurley, J. B., Baylor, D. A., & Simon, M. I. (1999). Abnormal photoresponses and light-induced apoptosis in rods lacking rhodopsin kinase. *Proceedings of the National Academy of Sciences of the United States of America*, **96**(7), 3718–3722.

Chen, C. K., Zhang, K., Church-Kopish, J., Huang, W., Zhang, H., Chen, Y. J., Frederick, J. M., & Baehr, W. (2001). Characterization of human GRK7 as a potential cone opsin kinase. *Molecular Vision*, **7**, 305–313.

Chen, J., Simon, M. I., Matthes, M. T., Yasumura, D., & LaVail, M. M. (1999). Increased susceptibility to light damage in an arrestin knockout mouse model of Oguchi disease (stationary night blindness). *Investigative Ophthalmology & Visual Science*, **40**(12), 2978–2982.

Dizhoor, A. M., & Peshenko, I. V. (2021). Regulation of retinal membrane guanylyl cyclase (RetGC) by negative calcium feedback and RD3 protein. *Pflugers Archiv: European journal of physiology*, **473**(9), 1393–1410.

Fadl, B. R., Brodie, S. A., Malasky, M., Boland, J. F., Kelly, M. C., Kelley, M. W., Boger, E., Fariss, R., Swaroop, A., & Campello, L. (2020). An optimized protocol for retina single-cell RNA sequencing. *Molecular Vision*, **26**, 705–717.

Fan, J., Rohrer, B., Moiseyev, G., Ma, J. X., & Crouch, R. K. (2003). Isorhodopsin rather than rhodopsin mediates rod function in RPE65 knock-out mice. *Proceedings of the National Academy of Sciences of the United States of America*, **100**(23), 13662–13667.

Frederiksen, R., Morshedian, A., Tripathy, S. A., Xu, T., Travis, G. H., Fain, G. L., & Sampath, A. P. (2021). Rod photoreceptors avoid saturation in bright light by the movement of the G protein transducin. *Journal of Neuroscience*, **41**(15), 3320–3330.

Frederiksen, R., Nymark, S., Kolesnikov, A. V., Berry, J. D., Adler, L., Koutalos, Y., Kefalov, V. J., & Cornwall, M. C. (2016). Rhodopsin kinase and arrestin binding control the decay of photoactivated rhodopsin and dark adaptation of mouse rods. *Journal of General Physiology*, **148**(1), 1–11.

Fu, Y., Kefalov, V., Luo, D. G., Xue, T., & Yau, K. W. (2008). Quantal noise from human red cone pigment. *Nature Neuroscience*, **11**(5), 565–571.

Fu, Y., & Yau, K. W. (2007). Phototransduction in mouse rods and cones. *Pflugers Archiv: European journal of physiology*, **454**(5), 805–819.

Govardovskii, V. I., Fyhrquist, N., Reuter, T., Kuzmin, D. G., & Donner, K. (2000). In search of the visual pigment template. *Visual Neuroscience*, **17**(4), 509–528.

Gulati, S., & Palczewski, K. (2023). Structural view of G protein-coupled receptor signaling in the retinal rod outer segment. *Trends in Biochemical Sciences*, **48**(2), 172–186.

Gurevich, V. V., Hanson, S. M., Song, X., Vishnivetskiy, S. A., & Gurevich, E. V. (2011). The functional cycle of visual arrestins in photoreceptor cells. *Progress in Retinal and Eye Research*, **30**(6), 405–430.

Ingram, N. T., Sampath, A. P., & Fain, G. L. (2019). Voltage-clamp recordings of light responses from wild-type and mutant mouse cone photoreceptors. *Journal of General Physiology*, **151**(11), 1287–1299.

Ishibashi, M., Keung, J., Morgans, C. W., Aicher, S. A., Carroll, J. R., Singer, J. H., Jia, L., Li, W., Fahrenfort, I., Ribelayga, C. P., & Massey, S. C. (2022). Analysis of rod/cone gap junctions from the reconstruction of mouse photoreceptor terminals. *eLife*, **11**, e73039.

Kawamura, S., & Tachibanaki, S. (2022). Molecular bases of rod and cone differences. *Progress in Retinal and Eye Research*, **90**, 101040.

Kolesnikov, A. V., Golobokova, E. Y., & Govardovskii, V. I. (2003). The identity of metarhodopsin III. *Visual Neuroscience*, **20**(3), 249–265.

Lamb, T. D. (2022). Photoreceptor physiology and evolution: Cellular and molecular basis of rod and cone phototransduction. *The Journal of Physiology*, **600**(21), 4585–4601.

Maeda, R., Hiroshima, M., Yamashita, T., Wada, A., Nishimura, S., Sako, Y., Shichida, Y., & Imamoto, Y. (2014). Single-molecule observation of the ligand-induced population shift of rhodopsin, a G-protein-coupled receptor. *Biophysical Journal*, **106**(4), 915–924.

© 2026 The Author(s). *The Journal of Physiology* published by John Wiley & Sons Ltd on behalf of The Physiological Society.

14697793, 2026, 22, Downloaded from https://physoc.onlinelibrary.wiley.com/doi/10.1113/JP291252 by University Of California Irvine Science Library Serials, Wiley Online Library on [18/11/2026]. See the Terms and Conditions (https://onlinelibrary.wiley.com/terms-and-conditions) on Wiley Online Library for rules of use; OA articles are governed by the applicable Creative Commons License

Makino, C. L., Wen, X. H., & Lem, J. (2003). Piecing together the timetable for visual transduction with transgenic animals. *Current Opinion in Neurobiology*, **13**(4), 404–412.

Mendez, A., Burns, M. E., Sokal, I., Dizhoor, A. M., Baehr, W., Palczewski, K., Baylor, D. A., & Chen, J. (2001). Role of guanylate cyclase-activating proteins (GCAPs) in setting the flash sensitivity of rod photoreceptors. *Proceedings of the National Academy of Sciences of the United States of America*, **98**(17), 9948–9953.

Nikonov, S. S., Brown, B. M., Davis, J. A., Zuniga, F. I., Bragin, A., Pugh, E. N., Jr., & Craft, C. M. (2008). Mouse cones require an arrestin for normal inactivation of phototransduction. *Neuron*, **59**(3), 462–474.

Nikonov, S. S., Kholodenko, R., Lem, J., & Pugh, E. N., Jr. (2006). Physiological features of the S- and M-cone photoreceptors of wild-type mice from single-cell recordings. *Journal of General Physiology*, **127**(4), 359–374.

Nymark, S., Frederiksen, R., Woodruff, M. L., Cornwall, M. C., & Fain, G. L. (2012). Bleaching of mouse rods: Microspectrophotometry and suction-electrode recording. *The Journal of Physiology*, **590**(10), 2353–2364.

Sakurai, K., Chen, J., & Kefalov, V. J. (2011). Role of guanylyl cyclase modulation in mouse cone phototransduction. *Journal of Neuroscience*, **31**(22), 7991–8000.

Sakurai, K., Chen, J., Khani, S. C., & Kefalov, V. J. (2015). Regulation of mammalian cone phototransduction by recoverin and rhodopsin kinase. *Journal of Biological Chemistry*, **290**(14), 9239–9250.

Sakurai, K., Onishi, A., Imai, H., Chisaka, O., Ueda, Y., Usukura, J., Nakatani, K., & Shichida, Y. (2007). Physiological properties of rod photoreceptor cells in green-sensitive cone pigment knock-in mice. *Journal of General Physiology*, **130**(1), 21–40.

Salido, E. M., & Ramamurthy, V. (2020). Proteoglycan IMPG2 shapes the interphotoreceptor matrix and modulates vision. *Journal of Neuroscience*, **40**(20), 4059–4072.

Sato, S., Jastrzebska, B., Engel, A., Palczewski, K., & Kefalov, V. J. (2019). Apo-Opsin exists in equilibrium between a predominant inactive and a rare highly active State. *Journal of Neuroscience*, **39**(2), 212–223.

Sato, S., Yamashita, T., & Matsuda, M. (2020). Rhodopsin-mediated light-off-induced protein kinase A activation in mouse rod photoreceptor cells. *Proceedings of the National Academy of Sciences of the United States of America*, **117**(43), 26996–-27003.

Sommer, M. E., & Farrens, D. L. (2006). Arrestin can act as a regulator of rhodopsin photochemistry. *Vision Research*, **46**(27), 4532–4546.

Sun, H., Macke, J. P., & Nathans, J. (1997). Mechanisms of spectral tuning in the mouse green cone pigment. *Proceedings of the National Academy of Sciences of the United States of America*, **94**(16), 8860–8865.

Vinberg, F., Chen, J., & Kefalov, V. J. (2018). Regulation of calcium homeostasis in the outer segments of rod and cone photoreceptors. *Progress in Retinal and Eye Research*, **67**, 87–101.

Vinberg, F., & Kefalov, V. (2015). Simultaneous ex vivo functional testing of two retinas by in vivo electroretinogram system. *Journal of visualized experiments: JoVE*, **99**, e52855.

Vinberg, F., Kolesnikov, A. V., & Kefalov, V. J. (2014). Ex vivo ERG analysis of photoreceptors using an in vivo ERG system. *Vision Research*, **101**, 108–117.

Vinberg, F., Wang, T., De Maria, A., Zhao, H., Bassnett, S., Chen, J., & Kefalov, V. J. (2017). The Na^+/Ca^{2+}, K^+ exchanger $NCKX_4$ is required for efficient cone-mediated vision. *eLife*, **6**, e24550.

Vinberg, F., Peshenko, I. V., Chen, J., Dizhoor, A. M., & Kefalov, V. J. (2018). Guanylate cyclase-activating protein 2 contributes to phototransduction and light adaptation in mouse cone photoreceptors. *Journal of Biological Chemistry*, **293**(19), 7457–7465.

Vogel, R., Siebert, F., Zhang, X. Y., Fan, G., & Sheves, M. (2004). Formation of Meta III during the decay of activated rhodopsin proceeds via Meta I and not via Meta II. *Biochemistry*, **43**(29), 9457–9466.

Wang, J. S., & Kefalov, V. J. (2010). Single-cell suction recordings from mouse cone photoreceptors. *Journal of visualized experiments: JoVE*, **35**, 1681.

Wen, X. H., Dizhoor, A. M., & Makino, C. L. (2014). Membrane guanylyl cyclase complexes shape the photoresponses of retinal rods and cones. *Frontiers in Molecular Neuroscience*, **7**, 45.

Woodruff, M. L., Lem, J., & Fain, G. L. (2004). Early receptor current of wild-type and transducin knockout mice: Photosensitivity and light-induced Ca^{2+} release. *The Journal of Physiology*, **557**(3), 821–828.

Xu, J., Dodd, R. L., Makino, C. L., Simon, M. I., Baylor, D. A., & Chen, J. (1997). Prolonged photoresponses in transgenic mouse rods lacking arrestin. *Nature*, **389**(6650), 505–509.

Yau, K. W., & Nakatani, K. (1985). Study of the ionic basis of visual transduction in vertebrate retinal rods. *Progress in Clinical and Biological Research*, **176**, 21–31.

Zhao, J., Yoneda, M., Takeyama, M., Inoue, Y., Kataoka, T., Ohno-Jinno, A., Isogai, Z., Iwaki, M., & Zako, M. (2008). Competitive binding of heparin with hyaluronan to a specific motif in SPACR. *Journal of Neurochemistry*, **107**(3), 823–831.

Zhao, J., Yoneda, M., Takeyama, M., Miyaishi, O., Inoue, Y., Kataoka, T., Ohno-Jinno, A., Isogai, Z., Kimata, K., Iwaki, M., & Zako, M. (2008). Characterization of a motif for specific binding to hyaluronan in chicken SPACR. *Journal of Neurochemistry*, **106**(3), 1117–1124.

Additional information

Data availability statement

The data are available from the corresponding author upon request.

© 2026 The Author(s). *The Journal of Physiology* published by John Wiley & Sons Ltd on behalf of The Physiological Society.

14697793, 2026, 22, Downloaded from https://physoc.onlinelibrary.wiley.com/doi/10.1113/JP291252 by University Of California Irvine Science Library Serials, Wiley Online Library on [18/11/2026]. See the Terms and Conditions (https://onlinelibrary.wiley.com/terms-and-conditions) on Wiley Online Library for rules of use; OA articles are governed by the applicable Creative Commons License

Competing interests

The authors declare no competing financial interests.

Author contributions

S.S. and V.J.K. contributed to the conception and design of this research. S.S. and R.F. performed experiments and analysed data. S.S., V.J.K., R.F. and A.P.S. wrote the manuscript. All authors approved the final version of the manuscript.

Funding

This work was supported by NIH grants EY035884 and EY035137 (V.J.K.), NIH EY029817 (A.P.S.), an unrestricted grant to the UCLA Department of Ophthalmology from Research to Prevent Blindness, and the Jules Stein Eye Institute Core NEI grant P30 EY00331. The authors acknowledge support to the Gavin Herbert Eye Institute at the University of California, Irvine, from an unrestricted grant from Research to Prevent Blindness and from NIH core grant P30 EY034070.

Acknowledgements

We thank Yilu Xie (Ocular Microanatomy Core, Centre for Translational Vision Research, UC Irvine) for technical support in histology analysis. We thank Dr Jeannie Chen from the University of Southern California for providing the *Gcaps*$^{-/-}$ and *Arr1*$^{-/-}$ animals. We thank Dr Janis Lem from Tufts University for providing the *Gnat1*$^{-/-}$ animals.

Generative AI statement

Generative AI tools were not used in the preparation of this article.

Keywords

arrestin, calcium feedback, photoreceptor cell, phototransduction, rod–cone coupling

Supporting information

Additional supporting information can be found online in the Supporting Information section at the end of the HTML view of the article. Supporting information files available:

Peer Review History
Supporting Information

© 2026 The Author(s). *The Journal of Physiology* published by John Wiley & Sons Ltd on behalf of The Physiological Society.

14697793, 2026, 22, Downloaded from https://physoc.onlinelibrary.wiley.com/doi/10.1113/JP291252 by University Of California Irvine Science Library Serials, Wiley Online Library on [18/11/2026]. See the Terms and Conditions (https://onlinelibrary.wiley.com/terms-and-conditions) on Wiley Online Library for rules of use; OA articles are governed by the applicable Creative Commons License